catalysts

MDPI

Article

Dendrimer-Stabilized Ru Nanoparticles Immobilized in Organo-Silica Materials for Hydrogenation of Phenols

Eduard Karakhanov [1,*], Anton Maximov [1,2], Anna Zolotukhina [1], Adila Mamadli [1], Anna Vutolkina [1] and Andrey Ivanov [2]

[1] Department of Petroleum Chemistry and Organic Catalysis, Moscow State University, Moscow 119991, Russia; max@ips.ac.ru (A.M.); anisole@yandex.ru (A.Z.); memmedli_edile@mail.ru (A.M.); annavutolkina@mail.ru (A.V.)

[2] A.V. Topchiev Institute of Petrochemical Synthesis, Russian Academy of Sciences, Moscow 119991, Russia; aoivanov@ips.ac.ru

* Correspondence: kar@petrol.chem.msu.ru; Tel.: +7-495-939-53-77

Academic Editors: Albert Demonceau, Ileana Dragutan and Valerian Dragutan
Received: 14 November 2016; Accepted: 2 March 2017; Published: 14 March 2017

Abstract: New hybrid catalysts based on Ru nanoparticles, encapsulated into poly(propylene imine dendrimers), immobilized into silica pores, were synthesized and examined for the hydrogenation of alkyl-substituted phenols. The corresponding alkyl-substituted cyclohexanols were presented as the major reaction products, while incomplete hydrogenation products appeared to be minor. A competition between the sterical factors of dendrimer-containing carriers and the electronic factors of substrate substituents influenced the hydrogenation rate of the alkyl-substituted phenols. The carrier structure was found to have a significant influence on both the physical and chemical properties of the catalysts and their hydrogenation activity. The synthesized hybrid catalysts appeared to be stable after recycling and could be re-used several times without significant loss of activity.

Keywords: phenols; hydrogenation; Ru nanoparticles; dendrimers; organo-silica materials

1. Introduction

Hydrogenation of phenol is still an important process in the petrochemical industry, being used to obtain cyclohexanone, the essential feedstock for the synthesis of adipic acid and caprolactam [1–3]. Hydrogenation products of substituted phenols are used as feedstock for synthesis of lubricants, additives to oils and fuels, surfactants, and perfumes. The significant importance of alkyl-substituted phenols hydrogenation can be seen nowadays, in view of lignocellulose treatment and bio-fuels production [4,5].

Hydrogenation of phenols may be carried out in the gaseous or in the liquid phase, in the presence of VIII group metals (Fe, Co, Ni, Ru, Rh, Pd, Ir, Pt), deposited onto carbon, silica or alumina [6–9]. For the first time hydrogenation of phenol in the liquid phase was carried out in 1903, using NiO as a catalyst [10]. Cyclohexanol was obtained as the only reaction product after 55 h. Gas-phase hydrogenation of phenol was realized in the same year, with cyclohexanol and cyclohexanone obtained as the main reaction products and benzene, cyclohexane, and cyclohexene as minor reaction products [11]. In industry gas-phase hydrogenation of phenol is carried out at 120–170 °C and hydrogen pressure of 0.3–5 MPa in the presence of Pd/Al_2O_3 catalyst [3,6,7,12–16]. This is the main process to obtain cyclohexanone from phenol. Mixed metal oxides and sulfides can also be used as catalysts, resulting in aromatic or alicyclic compounds [6,10].

Reaction rate and product distribution in the liquid-phase hydrogenation of phenol depend on several factors, such as nature of the metal, support and solvent; temperature, hydrogen pressure, and

the presence of acid or base additions [7]. Thus, the rate of phenol hydrogenation for carbon-supported catalysts was found to decrease in the order: Rh > Ru > Pd > Pt [9,17]. Pd catalysts appeared more selective to cyclohexanone in comparison with Ni, Pt, and Rh [7,18,19], while Ru catalysts were more selective to cyclohexanol [20]. The yield of cyclohexanol or cyclohexanone in the presence of hydrophilic heterogeneous catalysts (Pd/Al_2O_3, Pd/TiO_2) was found to depend on the phenol adsorption features: via the OH-group. It led to high selectivity on ketone, whereas adsorption of the whole aromatic ring favored cyclohexanol formation [21–23]. Base additives, such as CaO or MgO, in contrast, facilitated cyclohexanone formation with yield of 89%–98% [3,6,7,24–28].

The main disadvantage of Pd-based supported catalysts is the necessity of high temperatures and, as a consequence, of high power consumption for successful reaction performance. Rh and Ru catalysts allow the process to be carried out at temperatures below 100 °C, often resulting in cyclohexanol as the main product. They can be advantageously applied for hydrogenation of phenols with various structures [20,29]. RuO_2 proved a more active and stable catalyst for aromatic ring saturation, providing turnover frequency (TOF) of up to 1000 h^{-1} in terms of the substrate reacted [30].

Systems, based on metal nanoparticles, stabilized by polymeric or low-molecular organic ligands, dispersed in reaction medium, appear to be more efficient catalysts. Thus, nanoparticles, obtained from Rh complexes with water-soluble poly(acrylic acid), poly(ethylene imine), and poly(*N*-vinylpyrrolidone), demonstrated high activity in hydrogenation of phenol at 20–60 °C and 0.1–2.0 MPa of hydrogen [7,31–37]. By varying the reaction conditions and polymer nature, one can selectively obtain cyclohexanol or cyclohexanone.

Replacement of water by tetra-alkyl ammonium ionic liquid favored a significant increase in cyclohexanone selectivity, if Rh nanoparticles, stabilized by poly(acrylic acid), were used as a catalyst [38]. Herein, in the presence of cyclodextrine, the cyclohexanone formed was not further converted into cyclohexanol [39].

Nonetheless, metal nanoparticles dispersed in the reaction medium, in spite of their higher activity and ability to carry out the reaction under mild conditions, as well as classical homogeneous catalysts, cannot be effectively recycled [37,40]. To develop new effective hydrogenation catalysts, various attempts were undertaken [32,33,41].

Thus, Ru nanoparticles deposited on polystyrene were used for hydrogenation of phenol to cyclohexanol still in 1981 [42]. Yields, obtained there, were not high (50% after 20 h at 25 °C and 100% after 7 h at 80 °C) and comparable with those, reached in the presence of conventional Ru/C [28]. Later polyaromatic frameworks (PAFs), developed on a polystyrene basis, impregnated with Ru nanoparticles, were applied in water medium at 80 °C and 1 MPa of H_2 [43].

Ru nanoparticles, stabilized by poly(*N*-vinylpyrrolidone) (PVP), supported on γ-Al_2O_3 and exposed to microwave radiation in situ, appeared as good catalysts for selective hydrogenation of phenol to cyclohexanone (yield of 71% within 2 h), more active than conventional Ru/Al_2O_3 [44]. However it required much more severe reaction conditions (160 °C, 50 MPa of H_2) in comparison with homogeneous Ru/PVP catalyst [39]. At the same time, Ru nanocatalyst, based on poly(*N*-vinylpyrrolidone), chemically grafted on a silica surface, appeared very active in solvent-free hydrogenation of benzene, reaching quantitative conversions with TOF values up to 70,000 h^{-1} already for 20 min at 110 °C and 4–8 MPa of hydrogen [45].

Pd nanoparticles deposited onto mesoporous graphite nitride, effectively catalyzed phenol hydrogenation in water medium at ambient pressure over a wide range of temperatures (20–90 °C) [46]. A cyclohexanone yield of 99% can be obtained already at room temperature and maintained high, when the temperature rises.

Nanoparticles formed in situ from complexes of Rh, Ru, and Pd with poly(alkyl amines), immobilized in amorphous silica, were successfully applied for the hydrogenation of alkenes and dienes [47,48]. Pd nanoparticles, encapsulated in pores of mesopororus silica, such as SBA-15 or MCF (mesoporous cellular foam), with grafted poly(ethylene imine) (PEI) effectively catalyzed hydrogenation of diphenylacetylene under ambient conditions [49], significantly exceeding in their activity homogeneous Pd/PEI catalyst.

Another tendency is incorporation of various organic moieties into the structure of mesoporous silicas, allowing the so-called "organosilicas" [50–53] to be obtained, in which individual organic groups are covalently bonded to two or more Si atoms. Also these organic groups are able to form complexes with metal ions and stabilize nanoparticles. Such materials are excellent supports for designing new hybrid catalysts.

Promising blocks for the design of organosilica materials can be dendrimers, that are spherically symmetric globular macromolecules with a branched regular structure [54,55]. Earlier we proposed an approach for synthesis of efficient heterogeneous catalysts, suggesting preliminary cross-linking of poly(propylene imine) (PPI) or poly(amido amine) (PAMAM) dendrimers by various bifunctional agents, followed by metal nanoparticles impregnation (Scheme 1) [56–61]. The presence of amino and/or amido groups in such types of organic ligands provides effective complexation with metal ions, as well as immobilization of metal nanoparticles within a polymeric network. Thus, Ru catalysts, synthesized in such a way, demonstrated activity in hydrogenation of phenols and aromatics, essentially superior to conventional heterogeneous catalysts, at TOF values, exceeding 10,000 h^{-1} in some cases [57,58].

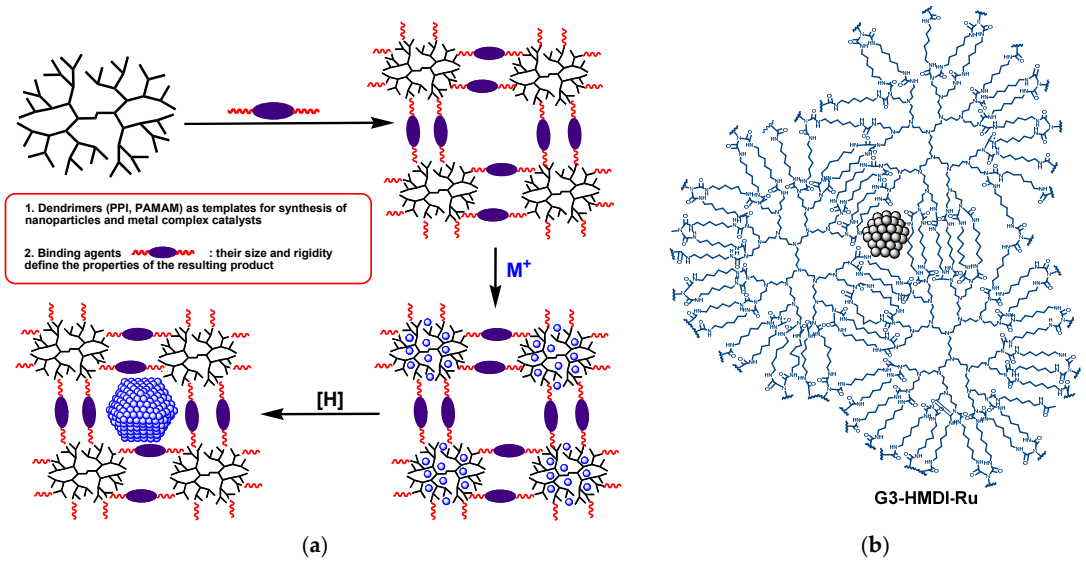

Scheme 1. (**a**) Approach for synthesis of nanoheterogeneous catalysts, based on dendrimer cross-linked networks [56–59,61]; (**b**) representative structure for Ru nanocatalysts, based on PPI dendrimers of the 3rd generation, cross-linked with hexamethylene diisocyanate (HMDI).

The main disadvantages of such materials are low porosity and exposure to hydrolysis under reaction conditions [57,62]. This problem can be solved by incorporation of dendrimers as bridged fragments into an organosilica structure, highly porous, with a high surface area.

Traditional hybrid catalysts, based on amorphous or mesoporous silica and PPI or PAMAM dendrimers, are synthesized via dendron immobilization onto the surface of ready carrier [41,63–70]. These materials are characterized by low dendrimer content and irregular dendrimer coating of the surface: anchoring of subsequent bulky dendrons is hindered due to diffusion limitations (bulky dendrons interfere with each other). As a consequence, this results in strictly limited metal content and irregular metal distribution through the carrier.

In the present work we propose an alternative approach for the synthesis of dendrimer-containing both amorphous and mesoporous organosilica materials by the sol-gel method, including co-hydrolysis of $Si(OEt)_4$ with PPI dendrimers, modified with (3-glycidoxy)propyltrimethoxysilane. Impregnated with Ru nanoparticles, these catalysts were applied for effective hydrogenation of phenols to the corresponding cyclohexanols.

2. Results and Discussion

2.1. The Synthesis of Heterogeneous Dendrimer-Based Catalysts

Modification of PPI dendrimers with (3-glycidoxypropyl)trimethoxysilane in ethanol medium, followed by acid-catalyzed $Si(OEt)_4$ hydrolysis and polymerization, resulted in ordered porous materials (Scheme 2). To obtain a mesoporous carrier, an aqueous solution of poly(ethylene glycol)-block-poly(propylene glycol)-block-poly(ethylene glycol) (Pluronic P123) was added preliminarily to a suspension of modified dendrimers (Scheme 3). In both cases dendrimers appeared as templates for pore formation (especially for microporous material, synthesized in the absence of polymer), as well as organic surface modifying ligands. Therefore they were not removed from the carrier structure, which is typical in a number of works, using dendrimers only as templates for regular pore formation and uniform particle size distribution [41,71–73]. Herein the sol-gel method allows diffusion limitations to be avoided, inevitable, when bulky dendrimer or dendron is anchored to the surface of ready carrier [64–69].

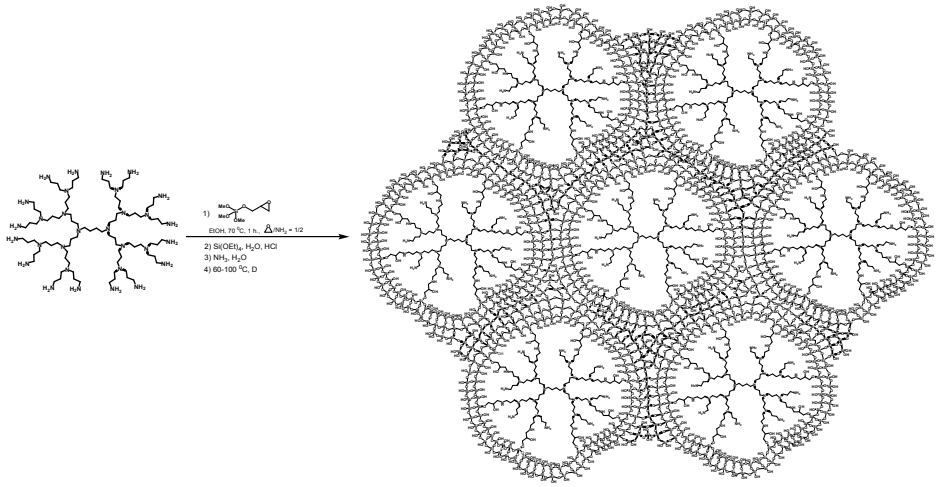

Scheme 2. The synthesis of hybrid G3-dendr-SiO_2 material.

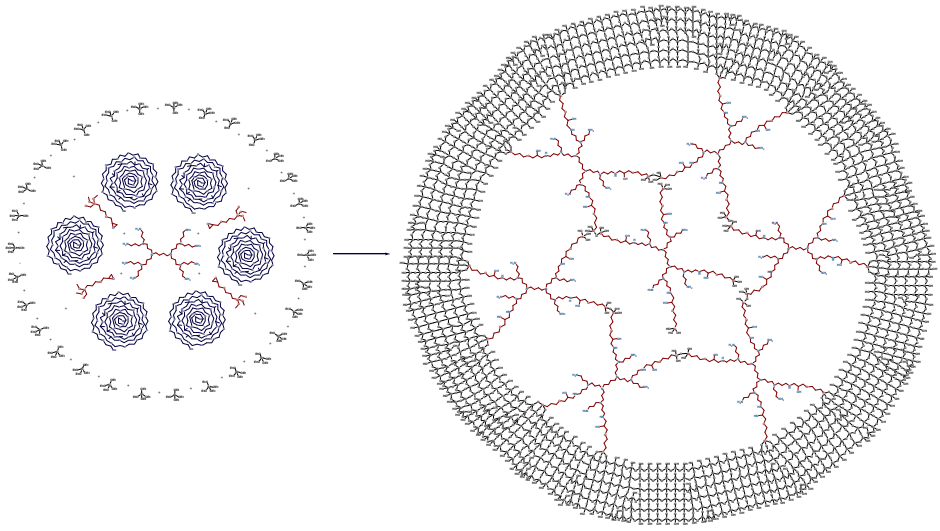

Scheme 3. The synthesis of hybrid G2-dendr-*meso*-SiO_2 material.

The materials obtained were characterized by infrared spectroscopy (IR), X-ray photoelectron spectroscopy (XPS) and solid-state nuclear magnetic resonance (NMR) spectroscopy, that confirmed

the presence in their structures of fragments, inherent in the SiO_2 bulk support [74,75], PPI dendrimers ($NCH_2CH_2CH_2N$, $NCH_2CH_2CH_2NH_2$, etc.) [76] and modifying groups, that link the former two residues, include epoxide-opening products of the former glycidyl groups ($SiCH_2CH_2CH_2O$, $OCH_2CH(OH)CH_2NH$) [76–80].

Transmission electron microscopy (TEM) and nitrogen low temperature adsorption and desorption (NLTAD) allowed differences in structures to be elucidated between these two types of hybrid supports. According to TEM data (Figure 1), dendr-G2-*meso*-SiO_2 support had a structure with straight hexagonal channels of SBA-15 type [53,66]. Herein the pore diameter was 5.5–7.5 nm. Microporous dendr-G3-SiO_2 (Figure 2) material was characterized by cell-like structure with channel size of 1.0–1.7 nm, that corresponded to the diameter of partly contracted PPI dendrimer of the 3rd generation.

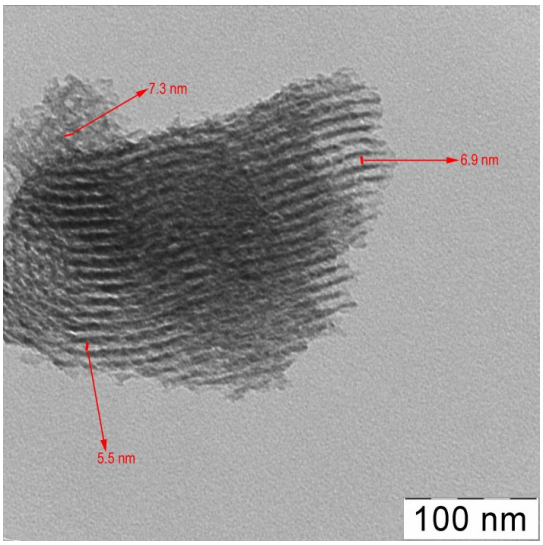

Figure 1. Transmission electron microscopy (TEM) microphotography of G2-dendr-*meso*-SiO_2 material.

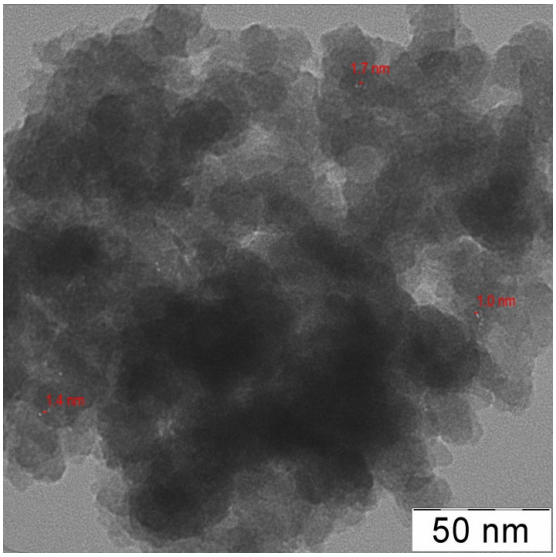

Figure 2. TEM microphotography of hybrid G3-dendr-SiO_2 material.

Data on the nitrogen low temperature adsorption and desorption for the synthesized hybrid materials are presented in Table S1. As seen from Table S1, dendr-G2-*meso*-SiO_2, prepared in the presence of template polymer, is much superior in its characteristics to microporous dendr-G3-SiO_2.

Adsorption average pore widths for both carriers are in accordance with those, obtained from the TEM data. Relatively low surface area for dendr-G2-*meso*-SiO_2, as compared with typical SBA-15 material [81] or that, modified by just small-size ligands [53,82], can be explained by dendrimers, that occupy a part of the pore space. However for dendr-G3-SiO_2 its very low cumulative surface area and pore volume may be connected not only with dendrimers, occupying the major part of the pore space, but also with the program interface, that takes into account pores more than 1.7 nm in diameter, i.e., more than the mean channel size, obtained from TEM.

The synthesis of metal nanoparticles, immobilized in the dendrimer-modified silica channels, was conducted by the wetness impregnation method (Scheme S1), according to procedures, described earlier in the literature [57]. $RuCl_3$ was deposited from aqueous solution at room temperature. Herein, in the presence of the grafted PPI dendrimer, complex formation of Ru with the amino-groups of dendrimers was a driving force, facilitating metal ion encapsulation and retention in silica pores. Ruthenium reduction was performed at room temperature, in water-ethanol medium, using $NaBH_4$ as reducing agent.

All the catalysts obtained were characterized by solid-state NMR spectroscopy, TEM, and XPS methods. Data are presented in Table 1 and in Figures 3, 4 and S1–S8. As one can observe, change in the carrier, from a microporous to a mesoporous one, results in a sufficient decrease of Ru content, that can be attributed both to larger pore diameter of G2-dendr-*meso*-SiO_2 and to decrease in the nitrogen donor coordination centers for G2-dendrimer vs. G3-dendrimer. Herein, mean particle size predictably increases (Table 1, Entries 1 and 2), being equal to 0.97 nm for microporous G3-dendr-SiO_2-Ru, that is typical for heterogeneous Ru catalysts, based on the PPI dendrimers of 3rd generation [57,58,83], and 1.28 nm for G2-dendr-*meso*-SiO_2-Ru.

Inclusion of Ru nanoparticles into silica pores, modified with grafted dendrimers did not destruct the mesoporous channel structure in G2-dendr-*meso*-SiO_2 (Figure 3), but resulted in the better peaks resolution in the ^{13}C NMR spectrum (Figure S1). Signals, corresponding to $OCH_2CH_2CH_2Si$ (8.7 ppm), $NCH_2CH_2CH_2N$ (23.3 ppm), $-CH_2CH_2OCH_2-$ (~73 ppm), and $-NCH_2O-$ (~84 ppm) fragments become well distinguishable. Indeed, wide pores in G2-dendr-*meso*-SiO_2 contain a sufficient amount of water, adsorbed on the silica walls or included between the dendrimer branches. Ru nanoparticles, when impregnated in pores, order water molecules around them, as well as dendritic aminogroups. Maintenance of the mesoporous structure for G2-dendr-*meso*-SiO_2-Ru was also confirmed by NLTAD resulting in reduction of surface area after metal encapsulation only by 15% and presented in additional TEM images (Figures S3 and S4). Similar results with an ordered silica structure not destroyed after metal encapsulation and following reduction in the presence of aqueous $NaBH_4$ were observed also in references [84–86].

G3-dendr-SiO_2-Ru is characterized by an ordered and compact nanoparticles arrangement (Figure 4)—in contrast to earlier described G3-HMDI-Ru (HMDI: hexamethylene diisocyanate), based on the polymeric network of 3rd generation PPI dendrimers, cross-linked with hexamethylene diisocycanate [57]. Their impregnation into silica pores did not result in any significant changes in ^{13}C NMR spectrum (Figure S2)—with respect to G2-dendr-*meso*-SiO_2-Ru (Figure S1). Signals, belonging to $OCH_2CH_2CH_2Si$ (9.2 ppm), $NCH_2CH_2CH_2N$ (23.6 ppm), $NCH_2CH_2CH_2N$ (52.4–53 ppm), and $-CH_2CH_2OCH_2-$ (73.6–75 ppm) fragments are well distinguishable both in the catalyst and initial carrier spectra (Figure S2) and located at the same positions. These data agree with those, described in the literature for silica, modified with simple O,N-coordinating organic ligands [52], as well as grafted polyalkylamines [87] and dendrimers [88]. Very small shifts take place only for CH_2 groups, attached directly to coordinating donor amino or ether groups. One may assume, that PPI dendrimers of the 3rd generation, acting both as modifying ligands and as a template during the synthesis of G3-dendr-SiO_2, occupy the major part of the free space in the pores of the corresponding hybrid support. As a consequence, this carrier contains less water, which could result in peak smearing and resolution loss. Also the structure of G3-dendr-SiO_2 with its thin pores, fitting in diameter with the dendrimers within, appears to be quite rigid, and Ru nanoparticles, when impregnated inside, cannot cause any sufficient changes in it, which may be reflected in the NMR spectrum.

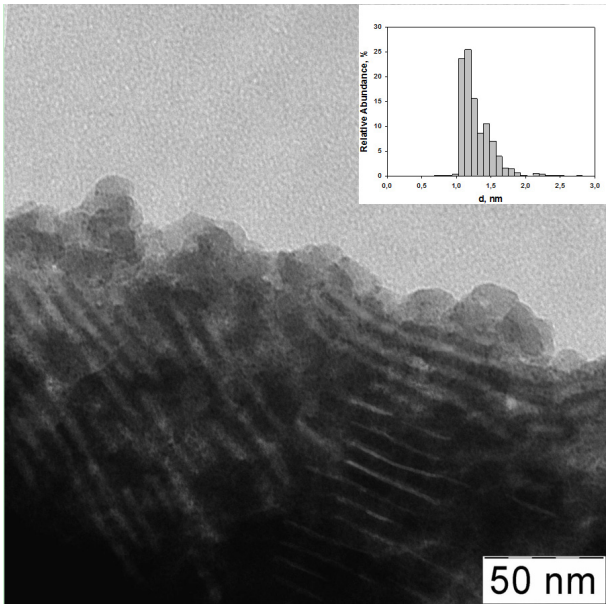

Figure 3. G2-dendr-*meso*-SiO_2-Ru catalyst: TEM microphotography and particles size distribution.

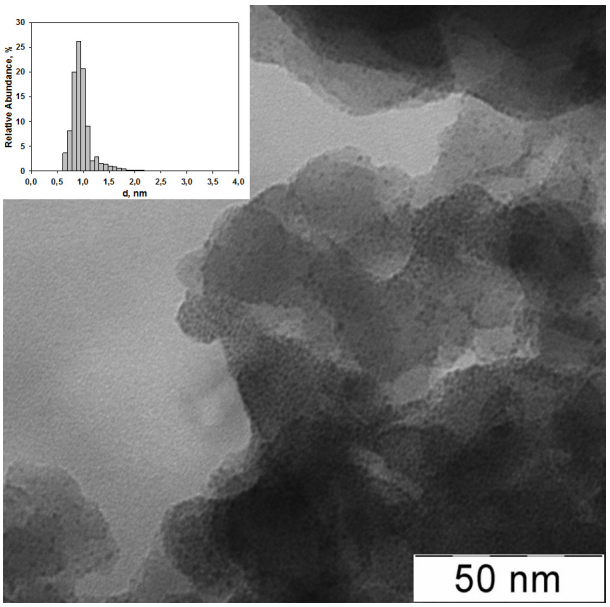

Figure 4. G3-dendr-SiO_2-Ru catalyst: TEM microphotography and particles size distribution.

As seen from XPS data (Table 1, Figures S5 and S6), metals in catalysts synthesized are presented in both zero-valent (Ru^0 [89], Ru/RuO_x [89]) and oxidized states (RuO_2 [90], RuO_3 [91], $RuCl_2$ [92], $RuCl_3$ [80]). Herein we suppose interaction of Ru nanoparticles with silica walls is minimal due to the preferential stabilization of the former by numerous aminogroups of PPI dendrimers inside pores, resulting in surface zero-valent forms for Ru nanoparticles. Oxidized forms such as RuO_2 or RuO_3 may be from interaction of Ru surface atoms with adsorbed water [93,94], while $RuCl_2$ and $RuCl_3$ forms may originate from incomplete reduction of initial $RuCl_3$ and present as surface complexes with aminogroups of dendritic ligands [90,92–95]. We suppose these data agree with those, obtained from solid-state NMR spectroscopy, and the stated above assumption, that Ru nanoparticles in G2-dendr-*meso*-SiO_2-Ru order water molecules around them. As a consequence, the percentage of Ru surface oxidized forms increases.

Table 1. Physical and chemical properties of the catalysts synthesized.

Entry	Catalyst	Ru (wt %)	*d* (nm)	Surface concentration by XPS (at. %)					Ru valency states at Ru $3p_{3/2}$ line (at. %)				
				Ru	C	N	O	Si	Ru^0 (eV)	Ru/RuO_x (eV)	RuO_2, Ru(II) N-bound (eV)	RuO_x/Ru, Ru(III) O,N-bound (eV)	$RuCl_3 \cdot xH_2O$, RuO_3 (eV)
1	G3-dendr-SiO_2-Ru	5.4	0.97 ± 0.09	4.2	22.1	4.5	55.9	13.3	32.7 (461.3)	-	50.2 (464.0)	-	17.1 (466.6)
2	G2-dendr-*meso*-SiO_2-Ru	3.5	1.28 ± 0.09	5.7	32.7	-	35.8	25.8	2.5 (460.5)	3.3 (462.2)	28.3 (463.6)	40.7 (465.0)	25.2 (466.4)

G2-dendr-*meso*-SiO_2-Ru, in spite of its lowest oxygen atomic concentration, demonstrates a high content of Ru-oxidized species (Table 2, Figure S5), which is also confirmed by deconvolution of O 1s spectra (Figure S5). $[Ru^0]/[RuO_x + Ru^{n+}]$ ratio makes up here 0.06 for G2-dendr-*meso*-SiO_2-Ru vs. 0.48 for G3-dendr-SiO_2-Ru. Also it should be taken into account, that, in spite of similar nitrogen loading in both carriers, PPI dendrimers of 2nd generation in G2-dendr-*meso*-SiO_2 carrier are more rarely located in wide pores and present less local concentration of donor aminogroups; as a result, Ru nanoparticles, due to their high affinity to oxygen [96–98], are not only easier oxidized on storage [99], but also may interact directly with the silica support, contributing to RuO_2 and RuO_3 species in both O 1s and Ru 3d spectra (Figure S7).

Table 2. Hydrogenation of phenol in water in the presence of G3-dendr-SiO_2-Ru catalyst [1].

Entry	Substrate/Ru (mol/mol)	*T* (°C)	*P* (MPa)	*t* (h)	Conv. (%)	TOF (H_2) (h^{-1})
1	377	85	3	0.5	94	1820
2	377	85	1	6	71	1172
3	377	70	3	6	100	3100
4	377	70	1	6	46	225
5	754	85	3	6	100	1853
6	754	85	1	6	32	212
7	887	80	3	6	99	1841

[1] Reaction conditions are: $m(PhOH) = V(H_2O)$.

The reverse situation is observed for G3-dendr-SiO_2-Ru, where small Ru particles (~1 nm) are located presumably inside of globules of sterically hindered dendrimers of the 3rd generation. As a consequence, the local ratio of ligand to metal is higher, and ruthenium nanoparticles are better stabilized, resulting in a higher portion of Ru^0 form in the Ru 3p spectrum (Table 1, Figure S6) and a lower contribution of Ru-O species in the O 1s spectrum (Figure S8).

2.2. Hydrogenation of Phenols in the Presence of Heterogeneous Dendrimer-Based Catalysts

The catalysts synthesized were examined in two-phase hydrogenation of phenols and its alkyl-substituted analogues. Herein substrate concentration was 1 mg or 1 μL per 1 μL of water, depending on the physical state of the former under ambient conditions, as in our previous works, dealing with two-phase Ru-catalyzed hydrogenation [57,58]. The use of water, in particular in a weight ratio to substrate of 1:1, promotes Ru catalysis, reaching a 10–1000-fold improvement in the reaction rate, which has already been proved by a series of works [57,100,101].

First of all, the influence of temperature, pressure, substrate/Ru ratio, and reaction time on reaction rate and product distribution on phenol hydrogenation was investigated. The results are presented in Tables 2 and 3 and in Figures 5 and 6. Catalyst activities (TOF (H_2)), expressed as turnover frequencies, were calculated in terms of hydrogen uptake by substrate per mole of ruthenium per hour according to the formula:

$$\mathrm{TOF}_{(H_2)} = \frac{\nu_{substr} \times \omega \times \nu_{H_2}}{\nu_{Ru} \times t} \quad (1)$$

where ω is substrate conversion, expressed in unit fractions. Hydrogen uptake was calculated as a sum of hydrogen moles, required e.g. for cyclohexanol and cyclohexanone formation, multiplied by corresponding selectivities, expressed in unit fractions, according to common reaction (Scheme 4):

The experimental reaction time, applied for TOF calculations, was such, that the hydrogenation kinetic curve had a maximum slope. In the majority of cases it was an area of 10–30 min with conversions of 20%–30% (Tables S2–S6). It should be noted, that carrying out the experiments for less reaction time (e.g., 5 min) results in incorrect evaluation of conversion and selectivity due to additional errors in time measurements as well as due to various physical chemical processes (homogenization of

local heat and reactant concentration through the volume, hydrogen adsorption, etc.), that have not enough time for equilibration to be established. Therefore we get lower estimated, but proven TOFs.

Table 3. Comparison of newly synthesized hybrid Ru catalysts with the earlier described materials, based on dendritic networks [57] [1].

Entry	Catalyst	Phenol/Ru (mol/mol)	*T* (°C)	Conv. (%)	TOF (H_2) (h^{-1})
1	G2-dendr-*meso*-SiO_2-Ru	1843	80	56	6090
2	G1–HMDI–Ru	910	85	61	2775
3	G3-dendr-SiO_2-Ru	887	80	66.5	1841
4	G3–HMDI–Ru	960	85	57	2745

[1] Reaction conditions: 30 min, 3 MPa of H_2, *m*(PhOH) = *V*(H_2O).

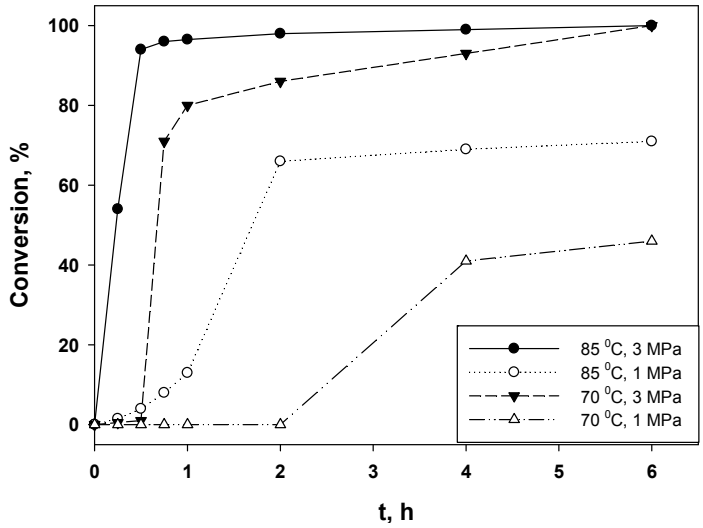

Figure 5. Kinetics of phenol hydrogenation in water in the presence of G3-dendr-SiO_2-Ru at substrate/Ru = 377. Reaction conditions are: *m*(PhOH) = *V*(H_2O).

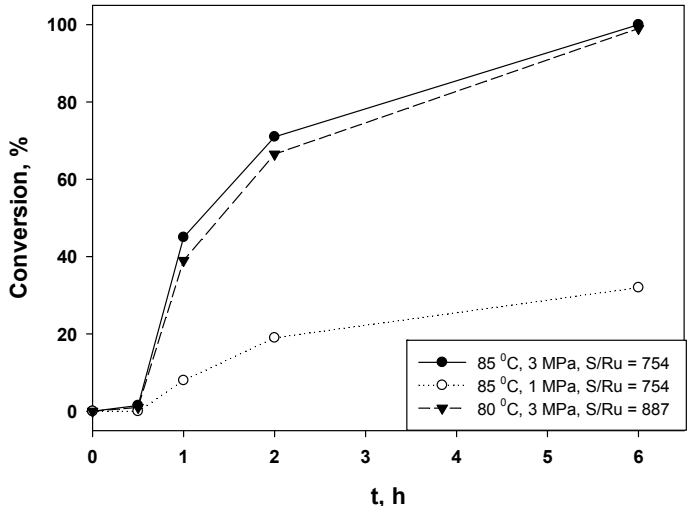

Figure 6. Kinetics of phenol hydrogenation in water in the presence of G3-dendr-SiO_2-Ru at substrate/Ru = 754–887. Reaction conditions are: *m*(PhOH) = *V*(H_2O).

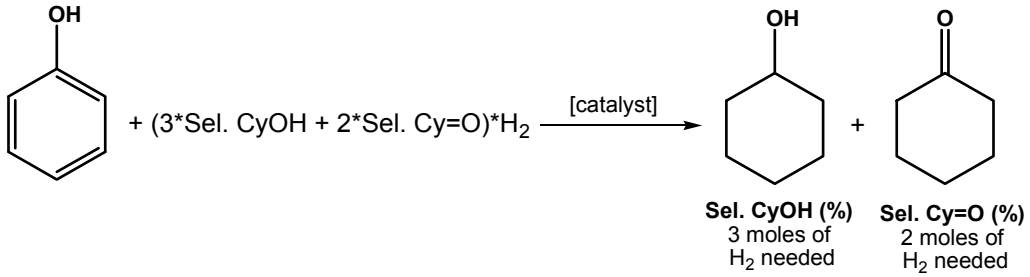

Scheme 4. Typical illustration for calculation of hydrogen consumed.

If an induction period took place (Figures 5 and 6), then the time interval with the maximum slope of the curve would be taken into account for the TOF calculation. Here the induction period was subtracted from the reaction time, for which noticeable conversions (~20%–30%) were observed.

As one can see, quantitative conversions of phenol become achievable already after 30 min at more severe reaction conditions and higher catalyst loadings (Figure 5, Table S2). A decrease in hydrogen pressure, as well as of temperature, results in an induction period of 0.5–1 h (Figure 5). A similar effect is caused by the increase in substrate/Ru ratio (Figure 6, Table S3). Nonetheless, quantitative conversions of phenol are still achievable over a period of 6 h (Table 2).

Herein the pressure affords the strongest influence on the catalyst's activity and, as a consequence, on the rate of phenol hydrogenation. Thus, at 70 °C and 1 MPa of hydrogen, conversion of phenol does not exceed 50% after 6 h with an induction period of 2 h (vs. 100% at 70 °C and 3 MPa of H_2) (Figure 5). Analogously it makes only 32% after 6 h at 85 °C and 1 MPa, when the substrate/Ru equal to 754 was used (vs. 100% at 3 MPa of H_2, all other conditions being equal) (Figure 6). Even at 85 °C and substrate/Ru = 377 conversion of phenol reaches only 71% within 6 h, rising slowly after 2 h (Figure 5).

Replacement of G3-dendr-SiO_2-Ru catalyst by its mesoporous analogue, that is G2-dendr-*meso*-SiO_2-Ru, resulted in disappearance of the induction period and an essential increase of the reaction rate, even at a much higher substrate/Ru ratio (Table S4, Figure 7). The phenomenon observed can be attributed to an open, less hindered structure of G2-dendr-*meso*-SiO_2 support, facilitating the substrate access to the catalytic centers, as well as to larger particle size (1.3 vs. 1 nm), providing a larger number of adsorption areas, which is especially remarkable at low pressures (Figure 7).

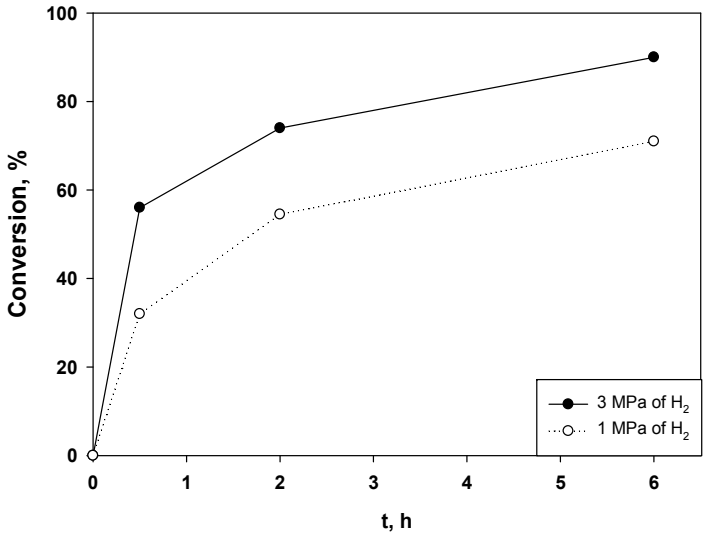

Figure 7. Hydrogenation of phenol in water in the presence of G2-dendr-*meso*-SiO_2-Ru. Reaction conditions are: S/Ru = 1843, at 80 °C, *m*(substr.) = *V*(H_2O).

In comparison with the earlier described materials, based on dendritic networks, with high reaction rates achieved, first of all, due to the high metal loading in the catalyst [57], the newly synthesized mesoporous hybrid catalyst appeared to be much more effective (Table 3). Thus, the turnover frequency for G2-dendr-*meso*-SiO_2-Ru at 80 °C and 3 MPa of hydrogen takes more than 6000 h^{-1} in terms of hydrogen uptake (Table S4) vs. 2775 h^{-1} for G1-HMDI-Ru and 2745 h^{-1} for G3-HMDI-Ru at 85 °C and all other conditions being equal [57]. G3-dendr-SiO_2-Ru, whose turnover frequency, as a rule, does not exceed 1850 h^{-1}, seems to be inferior not only to G1-HMDI-Ru, but also to the less active and more hindered G3-HMDI-Ru [57] (Table 3).

According to the XPS data, G3-dendr-SiO_2-Ru is characterized by lower surface metal content, as compared with G2-dendr-*meso*-SiO_2-Ru (Table 1) or G3-HMDI-Ru [57], which could result in a decrease of activity. At the same time, due to higher Ru0 atomic concentration (Table 1), G3-dendr-SiO_2-Ru does not have a crucial need for preliminary reduction to activate the catalytic centers. Hence the oxidation states of the Ru nanoparticles surface here are suggested to have less influence on the catalyst performance.

On the other hand, the increase in activity for Ru catalysts, based on dendritic networks, in water, was connected with partial destruction of the latter, caused by Ru-catalyzed hydrolysis of urethane bonds [57,62]. Vice versa, the catalyst, based on dendrimers of the 2nd generation, immobilized in meso-silica pores, proposed in the present work, appears less hindered. This circumstance facilitates access to the Ru centers not only for the substrate, but also for outside water molecules, that "activate" the Ru surface [100], resulting thereby in a sharp increase of reaction rate under the biphasic hydrogenation conditions [57,58].

The suggestion above is confirmed by results, obtained for microporous G3-dendr-SiO_2-Ru (Tables 2, 3, S2 and S3 and Figures 5 and 6). Small Ru nanoparticles, enclosed in narrow pores, in cages of hindered dendrimers of the 3rd generation, seem to have poor access to interaction with both substrate and outer water molecules. The latter, in spite of their small size, are retarded due to the multiple hydrogen bondsformation with amino groups of the 3rd generation PPI dendrimers, as well as with hydroxyl or ether groups of the former glycidyl fragments. As a consequence, the induction period appears, and a downfall in activity takes place, especially at reduced catalyst loadings, temperatures, and pressures.

Cyclohexanol was obtained as a major reaction product for both catalysts under all conditions being used: even at low conversions of phenol (~1%–5%) its part makes up at least 65% (Tables S2–S4). Nonetheless, the presence of cyclohexanone and 2-cyclohexanone among the reaction products sufficiently differentiates the synthesized hybrid catalysts from the earlier described G1-HMDI-Ru and G3-HMDI-Ru, based on cross-linked dendrimer networks, for which cyclohexanol was obtained as the only reaction product [57], while the results, as for G3-dendr-SiO_2-Ru and G2-dendr-*meso*-SiO_2-Ru (Tables S2–S4), were previously obtained for thermo-responsive Ru catalysts, based on poly(ethylene oxide) cross-linked PPI dendrimers of the 4th generation [61]. Thus, one may suppose, that donor amino-groups in the ruthenium nanoparticles microenviroment stabilize the cyclohexanone enol form (resulting in further hydrogenation of the latter) or facilitate its re-adsorption—in contrast to O-containing groups (that are widely presented in the dendr-SiO_2-Ru or PEG-dendr-Ru catalysts). As a consequence, the higher the amino-group concentration nearby to ruthenium nanoparticles, the higher the selectivity on cyclohexanol.

A similar tendency was observed for alkyl-substituted phenols (Tables S5 and S6). The main reaction products here were *cis*- and *trans*-isomers of corresponding substituted cyclohexanols. Their ratio was influenced by factors such as substrate size and substituent position relative to the hydroxyl group in the initial phenol molecule, as well as by the reaction time elapsed (Tables S5 and S6). Thus, the *cis*-fraction increased for large substrates, especially with substituents in the *ortho*-position (e.g., *o*-allyphenol, *p*-*tert*-butylphenol—Tables S5 and S6, Entries 5 and 6). *Cis*-isomer formation is preferentially in the literature, for both homogeneous [102] and heterogeneous catalysts [6,28,103,104], originating from syn-adsorption of the initial phenol molecule (Figure 8a) [103]. Trans-isomer formation

here is possible as a result of the rotation of the adsorbed enol form (Figure 8b), which is strongly affected by the substrate size and geometry [104]. Thus, large, bulky substituents, like *tert*-butyl, retard the rotation; which is also interfered with by substituents closely located to the OH-group, as in the *ortho*-position, resulting in preferential *cis*-isomer formation, as was already mentioned above [104].

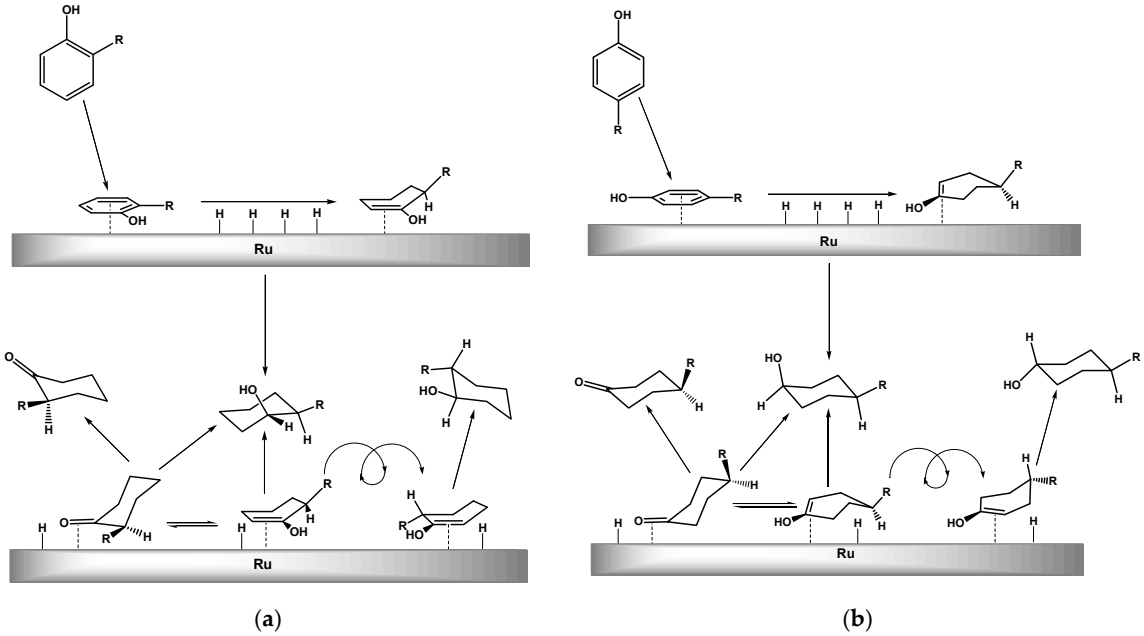

Figure 8. Possible ways for *cis*- and *trans*-product formation from *ortho*- and *para*-alkyl-substituted phenols. (**a**) *ortho*-isomers, (**b**) *para*-isomers.

Trans-isomers are thermodynamically more stable; as a consequence, their portion increases under thermodynamic reaction control, at long reaction times (2–6 h), which we can observe as an example of the results presented (Tables S5 and S6). The other factor, influencing trans-isomer formation, is the microenviroment of the catalytic centers, that can stabilize the enol form and facilitate its rotation. PPI dendritic moieties may appear as such a microenviroment as was already suggested in [57]. G1-HMDI and G3-HMDI networks contained about 40–50 wt % of dendrimer moieties, whereas for newly described G2-dendr-*meso*-SiO_2 and G3-dendr-SiO_2 porous hybrid carriers the dendrimer content is about only 15–20 wt %; as a result here, we obtain not only a lower hydrogenation rate for intermediate products, but also a lower conversion to *trans*-isomers.

Unsaturated intermediate hydrogenation products, such as alkylcyclohexanones and alkyl-2-cyclohexenones, were also detected (Tables S5 and S6). Their portion depended on reaction time, substrate as well as catalyst type, and reached maximum values for *p*-cresol (16.5%), *p*-ethylphenol (53%), *o*-allyphenol (43%), and *p*-*tert*-butylphenol (10%) within 0.5–1 h (Tables S6 and S7), especially when sterically more hindered and when less active G3-dendr-SiO_2-Ru was used (41%, 40.5%, 87%, and 30.5% correspondingly). Herein G3-dendr-SiO_2-Ru was again characterized by an induction period of 0.5 h for all substrates used. Also it should be noted, that in the case of *o*-allyphenol the C=C double bond in the side chain was first of all subjected to hydrogenation, and only then was the aromatic ring hydrogenated.

The presence of hydrogenolysis by-products (on both hydroxyl group and alkyl substituent, including subsequent hydrogenation) was characteristic for long reaction times: for cresols their part was especially high, reaching up to 20%–30% (Tables S5 and S6, Entries 1 and 2), gradually decreasing with substrate size increase. It should be noted, that hydrogenolysis is a common trend for Ru-based catalysts [6]. Thus, hydrogenolysis of alkylphenols and phenolic ethers was earlier reported in [57], while hydrolysis of alkanes was observed in [105].

Substrate size as well as substituent position to the hydroxyl group of the initial phenol, had a crucial effect on the catalyst's activity and reaction rate (Figure 9). A strong competition between sterical and electron factors took place, that earlier was observed for Ru containing dendritic networks [57]. Thus, there is a sharp downfall in both conversions and turnover frequencies, when phenol is replaced by *ortho*- or *para*-cresol. Such a pattern is typical for dendrimer-based systems and connected with the so-called negative dendritic effect, appearing as hindrance for large-sized, branched substrates to penetrate through the dendritic matrix [55,106,107]. Another side of the negative dendritic effect is the downfall in conversions, when the dendrimer generation increases [55,106,107], which one can see for G3-dendr-SiO_2-Ru, being inferior to G2-dendr-*meso*-SiO_2-Ru in the hydrogenation, not only of phenol itself, but also of its substituted analogues (Figure 9).

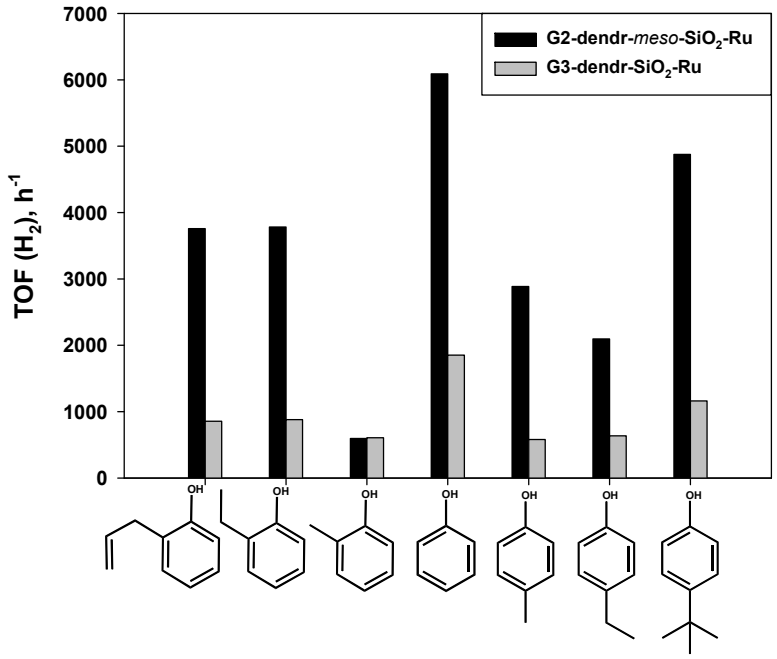

Figure 9. Hydrogenation of alkyl-substituted phenols in the presence of porous silica-immobilized dendrimer-based Ru catalysts. Reaction conditions are: at 80 °C, 3 MPa of H_2, V(substrate) = $V(H_2O)$.

Replacement of cresols by larger *ortho*-allyphenol or, especially, by *para-tert*-butylphenol, containing a substituent with a strong +*I*-effect, resulted in a sharp increase of activity for both catalysts: the latter reached comparable values of those for unsubstituted phenol (Figure 9). Herein dendritic moieties of the porous silica-based carriers did not contain hydrolysable bonds and therefore, as we assume, were not subjected to destruction, as were the earlier G1-HMDI and G3-HMDI dendritic networks [57]. Increase in activity for large substrates under these conditions may be explained in terms of dendrimers, that do not occupy all the free space in the silica pores—in contrast to dendritic networks with a high extent of cross-linking. Comparison of activities between newly synthesized hybrid catalysts, obtained by the sol-gel method, and earlier obtained based on dendrimer cross-linked networks [57], is presented in Table 4 and Table S7.

Table 4. Activities comparison for G1–HMDI–Ru [57] and G2-dendr-*meso*-SiO_2-Ru in the hydrogenation of alkyl-substituted phenols [1].

Entry	Substrate	Substrate/Ru (mol/mol) (G1–HMDI/ G2-dendr-*meso*-SiO_2)	*t* (h) (G1–HMDI/ G2-dendr-*meso*-SiO_2)	G1–HMDI–Ru		G2-dendr-*meso*-SiO_2-Ru	
				Conv. (%)	TOF (H_2) (h^{-1})	Conv. (%)	TOF (H_2) (h^{-1})
1	phenol	910/1843	0.5/0.5	61	2775	56	6090
2	*o*-cresol	960/1962	2/2	37	532	16.5	596
3	*p*-cresol	940/1905	2/0.5	20	282	29	2886
4	*o*-ethylphenol	967/1960	2/0.5	30	435	32.5	3728
5	*p*-ethylphenol	930/1890	0.5/0.5	31.5	1764	24	2097
6	*o*-allylphenol	980/2480	2/0.5	15	221	21	3759
7	*p*-*tert*-butylphenol	950/1922	0.5/0.5	45	2560	45	4879

[1] Reaction conditions are: at 85 °C G1–HMDI–Ru and at 80 °C for G2-dendr-*meso*-SiO_2-Ru, 3 MPa of H_2, *V*(substrate) = *V*(H_2O).

2.3. Catalyst Recycling

Synthesized hybrid catalysts, based on PPI dendrimers, immobilized into silica pores, were tested for the possibility of recycling in the hydrogenation of phenol in water medium. The recycling test was performed similarly to the standard procedure for hydrogenation in the presence of dendrimer-based ruthenium catalysts [57]. Ethanol was chosen as diluent for catalyst sedimentation due to its low viscosity and to avoid competitive adsorption, typical for acetone, which had already been demonstrated in [61]. Held for at least an hour, for better catalyst sedimentation, the resulting solution was decanted and new portions of phenol and water were added to the remaining catalyst. Eight reaction cycles were conducted in total for both catalysts. Results are presented in Figure 10.

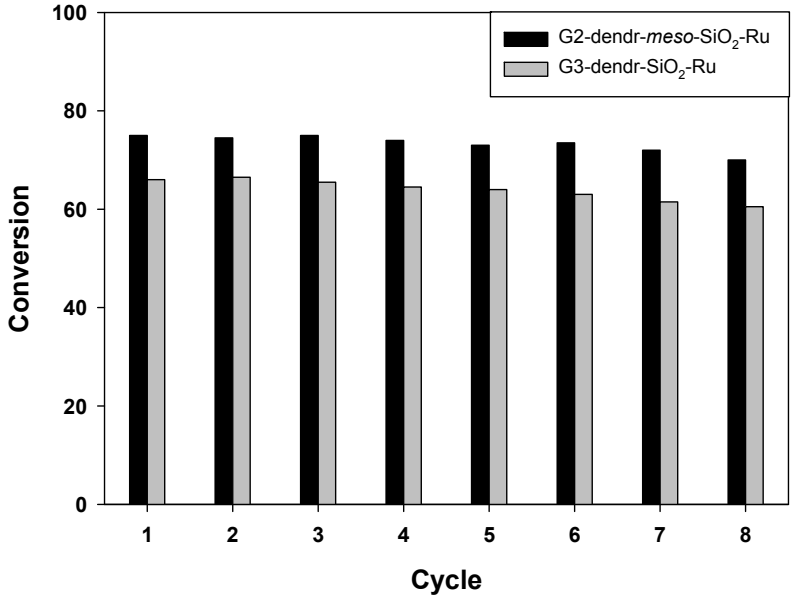

Figure 10. Recycling of porous silica-immobilized dendrimer-based Ru catalysts in phenol hydrogenation. Reaction conditions are: 5 mg of catalyst, 300 mg of phenol, 300 μL of water, at 80 °C, 3 MPa of H_2 for 2 h. PhOH/Ru ≈ 1843 for G2-dendr-*meso*-SiO_2-Ru and 887 for G3-dendr-SiO_2-Ru.

As seen from Figure 10, both G2-dendr-*meso*-SiO_2-Ru and G3-dendr-SiO_2-Ru appeared stable after recycling. Total turnover numbers for eight cycles were 32,460 for G2-dendr-*meso*-SiO_2-Ru and 13,362 for G3-dendr-SiO_2-Ru. According to ICP-AES, there was now metal leaching during recycling, and the slight decrease in activity can be explained by mechanical losses, which are inevitable on decantation.

3. Experimental

3.1. Chemicals

The following substances were used as substrates and reference compounds: phenol C_6H_5OH (Reachim, purum; Kharkov, Ukraine); cyclohexanol $C_6H_{11}OH$ (Ferak, Rein, Berlin, Germany); cyclohexanone $C_6H_{10}O$ (Jenapharm-Apolda, pro analysi; Jena, Germany); 2-cyclohexenone (Aldrich, ≥95%; Steinheim, Germany); *o*-cresol *o*-$CH_3C_6H_4OH$ (Reachim, purum); *p*-cresol *p*-$CH_3C_6H_4OH$ (Reachim, Purum); *o*-ethylphenol *o*-$C_2H_5C_6H_4OH$ (Acros Organics, 99%; St. Louis, MO, USA.); *p*-ethylphenol *p*-$C_2H_5C_6H_4OH$ (Reachim, Purum); *o*-allylphenol *o*-$C_3H_5C_6H_4OH$ (Aldrich, 98%); *p-tert*-butylphenol *p*-$(CH_3)_3CC_6H_4OH$ (Aldrich, 99%).

For the synthesis of mesoporous hybrid dendrimer-based catalysts the following were used: ruthenium(III) chloride $RuCl_3$ ("Aurat" OJSC, Purum, 47.80% of Ru content; Moscow, Russia), poly(propylene imine) (PPI) dendrimers of the 2nd (DAB$(NH_2)_8$) and 3rd generations (DAB$(NH_2)_{16}$) with a diaminobutane core (earlier prepared according to literature procedure [108]),

(3-glycidoxypropyl)trimethoxysilane (Acros Organics, ≥97%; Geel, Belgium), poly(ethylene glycol)-block-poly(propylene glycol)-block-poly(ethylene glycol) with the average number molecular weight Mn of 5800 $HO(CH_2CH_2O)_{20}(CH_2CH(CH_3)O)_{70}(CH_2CH_2O)_{20}H$ (Pluronic P123, Aldrich) and tetraethoxysilane $Si(OEt)_4$ (Aldrich, ≥99%).

3.2. Analyses and Instrumentations

Analysis by transmission electron microscopy (TEM) was conducted using a LEO912 AB OMEGA microscope (Carl Zeiss, Jena, Germany) with electron tube voltage of 100 kV. The count of particles and calculation of mean particle size was performed by processing the obtained micro-images using the "Image J" program.

X-ray photoelectron studies (XPS) were carried out using a LAS-3000 instrument (RIBER, Bezons, France), equipped with a photo-electronic analyzer with retarding potential OPX-150. To excite photoelectrons, aluminum anode X-ray radiation was used (Al Kα = 1486.6 eV) with a tube voltage of 12 kV and emission current of 20 mA. The calibration of photoelectron peaks was performed along the C1s line with binding energy of 284.8 eV.

Solid state ^{13}C Cross-Polarization Magic Angle Spinning (CPMAS) NMR spectroscopy analysis was carried out on the Varian NMR Systems 500 MHz spectrometer (Varian, Palo Alto, CA, USA) at an operating frequency of 125 MHz using TanCP with a spinning speed of 10 kHz.

FTIR spectra were registered with a Nicolet IR 2000 (Thermo Scientific, Madison, WI, USA) employing multiple distortion of the total internal reflection method with Multi-reflection HATR accessories, containing a ZnSe crystal 45° for different wavelengths with a resolution of 4 cm^{-1}.

Analysis by means of nitrogen low-temperature adsorption and desorption was carried out on a Gemini VII 2390 instrument (Micromeritics Instrument Corp., Norcross, GA, USA). Nitrogen adsorption–desorption isotherms were obtained at 77 K. The samples being analyzed were previously outgassed at 150 °C for 12 h. Surface area measurements were performed according to the Brunauer–Emmett–Teller (BET) method from nitrogen adsorption points in the range P/P_0 = 0.05–0.2. Pore size distribution was calculated using the Barrett–Joyner–Halenda model (BJH). The diameter corresponding to the maximum of the pore size distribution curve was suggested as the average pore size. Total pore volume was obtained at a relative pressure P/P_0 of 0.985.

Weight content of ruthenium in samples was determined with the help of a spectrophotometry method on the instrument "Agilent UV-Vis. 8453" (Agilent Technologies, Santa Clara, CA, USA) [109]. Ru-containing samples were treated with a mixture of 2 mL of concentrated hydrochloric acid (Sigma-Tech, Chemical Grade; Moscow, Russia) and 3 mL of 30% hydrogen peroxide (Aldrich). Then the solutions obtained were diluted with distilled water up to a volume of 10 mL, after that 15 mL of 0.015 M 1,10-phenantroline solution (Lachema, 98%; Brno, the Czech Republic) was added to them. To reduce Ru(III) to Ru(II), 0.2–0.6 g of hydroxylamine hydrochloride (Reachim, Purum) was added to each solution with a subsequent heating in a water bath at 100 °C for 2 h. After that all solutions were subjected to spectrophotometry analysis. Ruthenium content was determined by the intensity of the absorption band for the complex $[Ru(phen)_3]^{2+}$ at 449 nm ($\varepsilon = 1.5 \times 10^4$ $M^{-1} \cdot cm^{-1}$) [110].

Atomic emission spectroscopy with inductively coupled plasma was used to measure Ru leaching at the recycling tests with a help of an IRIS Interpid II XPL instrument (Thermo Electron Corp., Waltham, MA, USA) in radial and axial observation modes at wavelengths of 204.5 and 85.1 nm.

Qualitative and quantitative analyses of the reaction products were performed using a ChromPack CP9001 gas chromatograph (ChromPack, Amsterdam, the Netherlands) equipped with a flame ionization detector and a 30 m × 0.2 mm column containing a grafted SE-30 phase. Chromatograms were recorded and analyzed on a computer using the program Maestro 1.4. Conversion was calculated by changes in the relative area (%) of substrate and products peaks.

3.3. Synthetic Procedures for the Dendrimer-Based Catalysts

3.3.1. The Synthesis of Microporous G3-Dendr-SiO_2 Hybrid Support

Into a 10 mL single-neck round-bottom flask, equipped with a magnetic stirrer and a reflux condenser, 1.04 g (0.617 mmol) of DAB$(NH_2)_{16}$ dendrimer and 5 mL of ethanol were placed. Then, after the dendrimer had been completely dissolved in ethanol, 1.5 mL (6.8 mmol) of (3-glycidoxypropyl)triethoxysilane was added dropwise at room temperature, while stirring. Therefore there was one epoxy group of modifier for two end amino groups of the dendrimer. Reaction was carried out at 70 °C for one hour, while stirring. Herein the reaction mixture gradually thickened and later turned into a white flake-like gelatinous precipitate.

Then a preliminary homogenized mixture of 10 mL (45.121 mmol) of $Si(OEt)_4$ and 2 mL of aqueous (36%) hydrochloric acid was added to the product obtained. After a short time of stirring, a white gelatinous residue was formed. The mixture obtained was transferred into a chemical glass beaker, and after that 2 mL of aqueous (25%) ammonia and 5 mL of water were added to it. The white homogeneous gel formed was stored in a drying chamber for 3 h under a gradual temperature increase from 60 to 110 °C. The yield of the product obtained (as white powder) was 4.8 g (88%).

IR (cm^{-1}): 3446.70 (O-H_{st} and N-H_{st} NH-C(-OH), broad unresolved band); 2940 (C-H_{st}); 2927.73 (C-H_{st}, CH_2-O_{st}); 2845 (C-H_{st}, CH_2-N_{st}); 1750 (C=O_{st} in CH_2-C(=O), weak band); 1666.48 (C=O_{st} in CH_2-C(=O ... H), weak band; NH_{2d}); 1539.64 (NH_{2d}); 1465.15 (CH_{2d}); 1325, 1200, 1070.46 (C-O_{st}, C-N_{st} in NH-C(-OH)); 958.68; 799.85 (O-H_d); 750 (N-H_d, CH_{2g}, weak unresolved band).

XPS (eV): 103.2 (SiO_2, Si 2p, 19.5%); 285.7 ($NCH_2CH_2CH_2N$, NCH_2CH_2O, C 1s, 24.3%); 399.3 ($NCH_2CH_2CH_2N$, NCH_2CH_2O, N 1s, 5.1%); 532.7 (SiO_2, OCH_2CH_2O, O 1s, 51.1%).

^{13}C NMR (δ, ppm): 75 (-$CH_2CH_2OCH_2$); 66 (-$(CH_2)_2CHOH$); 58 ($NCH_2CH_2CH_2CH_2N$); 53 ($NCH_2CH_2CH_2N$); 46 ($NCH_2CH_2CH_2NHCH_2$); 38.5 ($NCH_2CH_2CH_2NH_2$); 23.6 ($NCH_2CH_2CH_2N$); 18.5 ($SiCH_2CH_2CH_2O$); 9.2 ($SiCH_2CH_2CH_2O$).

3.3.2. The Synthesis of Mesoporous G2-Dendr-*meso*-SiO_2 Hybrid Support

The synthesis of mesoporous dendrimer-based material was performed according to the following procedure [50]. Into a 25 mL single-neck round-bottom flask, equipped with a magnetic stirrer and a reflux condenser, 1.445 g (1.87 mmol) of DAB$(NH_2)_8$ dendrimer and 5 mL of ethanol were placed. Then 1.65 mL (7.5 mmol) of (3-glycidoxypropyl)triethoxysilane was added dropwise at room temperature, while stirring. Reaction was carried out at 80 °C for 2 h while stirring and the flask contents gradually turned into a viscous red oil. This reaction mixture was kept for a night at room temperature, after that it turned into a rose-orange gel, which was further evaporated on a rotary evaporator, giving a glass-like fragile residue, weighing 3.3 g. Therefore the first stage of synthesis was similar to the previously described procedure.

For the next stage, 1.46 g of Pluronic P123 was placed into a 100 mL glass beaker, containing a solution of 52.5 mL of deionized water and 0.325 mL of concentrated hydrochloric acid (Sigma-Tech, Chemical Grade). The mixture obtained was subjected to stirring at 50 °C for 3 h, gradually growing turbid. After that the previously obtained and ground modified dendrimer was added to the resultant colloid solution of polymer, followed by stirring for 2 h.

Then 1.6 mL of concentrated hydrochloric acid (Sigma-Tech, Chemical Grade) was added to 8.3 mL (37.2 mmol) of $Si(OEt)_4$, placed into a 25 mL glass beaker. This solution was added to the earlier obtained mixture of Pluronic P123 and $Si(OEt)_3$-modified dendrimer. Therefore, one mole of end modified amino groups of the dendrimer came into contact with 5 moles of $Si(OEt)_4$. A viscous milky-white mixture formed, which did not gelate for a night. This residue was stored in a drying chamber for 3 h with a gradual temperature increase from 60 to 110 °C, and after that it was subjected to stirring with 50 mL of water and 75 mL of ethanol at 70 °C, to wash out the polymer. Then 2 mL of aqueous ammonia (25%) and 5 mL of water were added, resulting in a white fluffy precipitate. After that, 2 mL of concentrated hydrochloric acid (Sigma-Tech, Chemical Grade) and 5 mL of water were

added. After one night the residue obtained was subjected to centrifugation, washed out with water and ethanol and dried in the air. The product was isolated as a cream powder, weighing 7.72 g.

^{13}C NMR (δ, ppm): 86 (-OCH_2N-); 74 (-CH_2CH_2O); 44 ($NCH_2CH_2CH_2N$); 30 ($NCH_2CH_2CH_2N$); 16 ($SiCH_2CH_2CH_2O$).

3.3.3. The Synthesis of Catalyst G2-Dendr-*meso*-SiO_2-Ru

The synthesis was performed according to the following procedure [57,108]. A 500 mg portion of the meso-DAB-PPI-G2-GlycdSiO_2 hybrid support, 10 mL of the distilled water, and 99 mg (0.48 mmol) of $RuCl_3$ were placed into a one-neck 50 mL round-bottom flask, equipped with a reflux condenser and a magnetic stirrer. Then another 5 mL of water was added. The reaction was carried out for 8 h at room temperature, while stirring. After that the reaction mixture was evaporated on a rotary evaporator, giving a dark-grey powder residue, weighing 441 mg (73.6%).

To reduce Ru(III) to Ru(0), 5 mL of aqueous solution of $NaBH_4$ (70 mg, 1.85 mmol) was added dropwise to a suspension of catalyst precursor (441 mg) in 5 mL of ethanol, while stirring. Then an additional 5 mL of ethanol was passed through the dropping funnel to wash the $NaBH_4$ residues down into the reaction mixture. Herein violent effervescence was observed. The reaction was conducted for 8 hours at room temperature, while stirring. After that, the suspension was centrifuged, and the residue was washed with water and ethanol, in order to separate from the soluble unreacted $NaBH_4$ and its oxidation product $Na_2B_4O_7$, and then dried in the air. The product was isolated as black-grey powder with a yield of 400 mg (66.8%).

ω_{Ru} (UV-Vis): 3.5%.

XPS (eV): 103.2 (SiO_2, Si 2p, 25.8%); 280.2 (Ru^0, Ru/RuO_x and RuO_2, Ru(II) N-bound, Ru $3d_{5/2}$), 281.7 ($RuCl_3$ or RuO_2, Ru $3d_{5/2}$), 282.4 (RuO_x/Ru or $RuCl_3 \cdot xH_2O$, Ru $3d_{5/2}$), 283.0 (RuO_3, Ru $3d_{5/2}$); 284.2 (Ru^0, Ru/RuO_x and RuO_2, Ru(II) N-bound, Ru $3d_{3/2}$), 285.8 ($RuCl_3$ or RuO_2, Ru $3d_{3/2}$), 286.7 (RuO_x/Ru or $RuCl_3 \cdot xH_2O$, Ru $3d_{3/2}$), 287.2 (RuO_3 or Ru(III/IV) O,N-bound, Ru $3d_{3/2}$); 283.7 (C-Si or C=M, C 1s, 6.9%), 285.0 ($NCH_2CH_2CH_2N$ and $SiCH_2CH_2CH_2O$, C 1s, 15.1%), 286.2 ($NCH_2CH_2CH_2N$, -$CH_2CH_2N \rightarrow Ru^0$, NCH_2CH_2O, OCH_2CH_2O, C 1s, 6.8%), 287.6 (O-C-O, -$CH_2CH_2O \rightarrow RuO_x$, C 1s, 3.0%), 288.9 (O-C-O, C 1s, 0.8%); 460.5 (Ru^0, Ru $3p_{3/2}$, 0.1%), 462.2 (RuO_2, Ru(II) N-bound, Ru $3p_{3/2}$, 0.2%), 463.6 ($RuCl_3$, Ru $3p_{3/2}$, 1.6%), 465.0 (RuO_x/Ru or $RuCl_3 \cdot xH_2O$, Ru $3p_{3/2}$, 2.3%), 466.4 (RuO_3 or Ru(III/IV) O,N-bound, Ru $3p_{3/2}$, 1.4%); 530.8 (RuO_x, O 1s, 19.0%), 532.6 (SiO_2, O-Si-CH_2, OCH_2CH_2O, O 1s, 16.8%).

^{13}C NMR (δ, ppm): 84 (-OCH_2N-); 73 (-CH_2CH_2O); 65 (-$(CH_2)_2CHOH$); 51 ($NCH_2CH_2CH_2N$); 23.3 ($NCH_2CH_2CH_2N$); 8.7 ($SiCH_2CH_2CH_2O$).

3.3.4. The Synthesis of Catalyst G3-Dendr-SiO_2-Ru

The synthesis of hybrid DAB-PPI-G3-GlycdSiO_2-Ru was performed according to the above described procedure [57,111]. An amount of 500 mg of a microporous hybrid carrier DAB-PPI-G3-GlycdSiO_2 and 94 mg (0.45 mmol) of $RuCl_3$ in 15 mL of water were taken as initial substances. The intermediate product was isolated as a dark-grey powder, weighing 563 mg (yield of 95%).

At the next step, 563 mg of the earlier obtained precursor and 171 mg (4.5 mmol) of $NaBH_4$ in a mixture of 5 mL of water and 10 mL of ethanol were taken to reduce Ru(III) to Ru(0). $NaBH_4$ was added here portion-wise, and self-heating of the reaction mixture was observed. The product obtained was isolated as a dark-grey powder with a yield of 539 mg (99%).

ω_{Ru} (UV-Vis): 5.4%.

XPS (eV): 103.0 (SiO_2, Si 2p, 13.3%); 278.2 (Ru^0, Ru $3d_{5/2}$, 1.35%), 281.1 (RuO_2 or $RuCl_2$ N-bound, Ru $3d_{5/2}$, 2.1%), 282.7 (RuO_3 or $RuCl_3$ N-bound, Ru $3d_{5/2}$, 0.7%), 283.2 (Ru^0, Ru $3d_{3/2}$), 285.2 (RuO_2 or $RuCl_2$ N-bound, Ru $3d_{3/2}$), 286.9 (RuO_x/Ru or $RuCl_3 \cdot xH_2O$, Ru $3d_{3/2}$); 283.5 (C-Si or C=M or C≡N, C 1s, 3.3%), 285.7 ($NCH_2CH_2CH_2N$, $SiCH_2CH_2CH_2O$, $NCH_2CH_2CH_2N$, -$CH_2CH_2N \rightarrow Ru^0$, -$CH_2CH_2N^+$, C 1s, 13.0%), 287.8 (O-C-O, O-C-N, $OCH_2CH_2N^+$, $CH_2CH_2O \rightarrow RuO_x$, C 1s, 5.0%), 289.6 (-$C(OCH_2$-$)_3$ or $NCH_2CH_2CH_2N/OCH_2CH_2O$ (sat), C 1s, 0.6%); 461.3 (Ru^0, Ru $3p_{3/2}$), 464.0

(RuO_2 or $RuCl_2$ N-bound, Ru $3p_{3/2}$), 466.6 (RuO_x/Ru or $RuCl_3 \cdot xH_2O$, Ru $3p_{3/2}$); 397.8 ($N{\equiv}Ru_{ads}$ or $-CH_2C{\equiv}N \rightarrow$ Ru or C=N-C, N 1s, 1.6%), 400.0 ($NCH_2CH_2CH_2N$, NCH_2CH_2O, $-CH_2N \rightarrow$ Ru, N 1s, 1.9%), 402.8 (NR_4^+, $R_3N^+ \rightarrow O^-$, N 1s, 1.0%); 531.4 (RuO_3, RuO_x/Ru, O 1s, 12.6%), 532.9 (SiO_2, O-Si-CH_2, OCH_2CH_2O, O 1s, 29.3%), 534.5 ($RuCl_3 \cdot xH_2O$, H_2O–N/H_2O–O, O 1s, 13.9%).

^{13}C NMR (δ, ppm): 73.6 ($-CH_2CH_2OCH_2$); 66 ($-(CH_2)_2CHOH$); 57 ($NCH_2CH_2CH_2CH_2N$); 52.4 ($NCH_2CH_2CH_2N$); 46 ($NCH_2CH_2CH_2NHCH_2$); 38.5 ($NCH_2CH_2CH_2NH_2$); 23.6 ($NCH_2CH_2CH_2N$); 9.2 ($SiCH_2CH_2CH_2O$).

3.4. Protocol for the Catalytic Experiments

The desired amounts of catalyst, substrate, and water were placed into a steel thermostated autoclave, equipped with a glass vial insert and a magnetic stirrer. Herein the substrate concentration was 1 mg (if the substrate was solid or powder) or 1 μL (if the substrate was liquid) per 1 μL of water. The autoclave was sealed, filled with hydrogen up to a pressure of 3 MPa, and connected to the thermostat. Reactions were conducted at 80 and 120 °C. After reaction for the required time, the autoclave was cooled down below room temperature and depressurized. Reaction products were analyzed by gas-liquid chromatography.

Activity of the catalysts (TOF = turnover frequency) was calculated as the amount of reacted substrate (ν_{substr}) per mole of metal (ν_{Ru}) per unit of time with account of the hydrogen uptake by the substrate:

$$TOF_{(H_2)} = \frac{\nu_{substr} \times \omega \times \nu_{H_2}}{\nu_{Ru} \times t} \quad (1)$$

where ω is substrate conversion, expressed in the unit fractions. Herein t is the minimal reaction time, for which the reaction progress is measured. If an induction period took place, it was subtracted from the minimal reaction time, characterized by any noticeable conversion.

The re-use of dendrimer-based Ru hybrid catalysts was conducted as follows. Catalyst (5 mg), phenol (300 mg) and water (300 μL) were placed into the steel thermostated autoclave equipped with a glass vial insert and a magnetic stirrer. The autoclave was sealed, filled with hydrogen up to a pressure of 3 MPa and then connected to the thermostat. The reaction was carried out for 2 h at 80 °C. After that, the reactor was cooled down below the room temperature and depressurized. The reaction mixture was diluted with ethanol (2 mL) and allowed to stand. Then, after visible catalyst particles had sedimented, the resulted solution was separated from the catalyst by decantation and analyzed by gas–liquid chromatography. The catalyst remaining in the vial was used for the next reaction cycles without additional loading, drying or regeneration.

4. Conclusions

In summary, new organosilica hybrid catalysts based on Ru nanoparticles, encapsulated into poly(propylene dendrimers) and immobilized into silica pores, were synthesized using a sol-gel method. Both catalysts proved their efficiency in the hydrogenation of various phenols, appearing stable under two-phase conditions and not subjected to hydrolysis, which was a characteristic of earlier described Ru catalysts, based on cross-linked dendrimer networks. The main products were the corresponding substituted cyclohexanols. Change in the hydrogenation rate depended on competition between sterical factors of the dendrimer-containing carrier and electronic factors of substrate substituents, similar to those earlier observed for Ru catalysts, based on cross-linked PPI-dendrimers.

The carrier structure was found to have a significant influence on both the catalysts physical chemical properties as well as their activity in the hydrogenation of phenols. Thus, mesoporous catalyst G2-dendr-*meso*-SiO_2-Ru, prepared in the presence of a polymer template, was characterized by the high percentage of surface oxidized forms of Ru, which may be due to the water adsorbed or ready exposure to oxidation on storage. This catalyst demonstrated the highest activity in the hydrogenation of phenol, as well as of its alkyl-substituted analogues (especially of *para-tert*-butyl-phenol), exceeding that, earlier described for G1-HMDI-Ru or other heterogeneous Ru-based catalysts.

In the case of microporous G3-dendr-SiO_2-Ru catalyst, having a more rigid structure than G2-dendr-*meso*-SiO_2-Ru, metal nanoparticles did not result in any sufficient changes in the structure and physical chemical properties of the initial carrier, when impregnated. In spite of a higher metal content and a much lower percentage of Ru surface oxidized forms, the catalyst G3-dendr-SiO_2-Ru was inferior to the mesoporous G2-dendr-*meso*-SiO_2-Ru. In the hydrogenation of phenols it was characterized by an induction period of 0.5–1 h, which might be due to substrate retarded access to the Ru catalytic centers. Synthesized hybrid catalysts, based on PPI dendrimers, immobilized into silica pores, appeared to be stable after recycling and can be re-used several times without significant loss of activity.

Supplementary Materials: The following are available online at www.mdpi.com/2073-4344/7/3/86/s1, Scheme S1: Encapsulation of Ru nanoparticles into PPI dendrimers, immobilized in silica pores. Figure S1: ^{13}C MAS NMR spectra of G2-dendr-*meso*-SiO_2-Ru catalyst and its carrier, Figure S2: ^{13}C MAS NMR spectra of G3-dendr-SiO_2-Ru catalyst and its carrier, Figure S3: Maintenance of mesoporous structure in G2-dendr-*meso*-SiO_2-Ru after reduction by aqueous $NaBH_4$, Figure S4: An overview TEM image of G2-dendr-*meso*-SiO_2-Ru, Figure S5: XPS spectrum of G2-dendr-*meso*-SiO_2-Ru, Ru 3p line, Figure S6: XPS spectrum G3-dendr-SiO_2-Ru, Ru 3p line, Figure S7: XPS spectrum of G2-dendr-*meso*-SiO_2-Ru, O 1s line, Figure S8: XPS spectrum G3-dendr-SiO_2-Ru, O 1s line, Table S1: Porosity properties of dendrimer-based hybrid materials according to nitrogen low temperature adsorption and desorption, Table S2: Hydrogenation of phenol in water in the presence of G3-dendr-SiO_2-Ru catalyst under various conditions at substrate/Ru of 377, Table S3: Hydrogenation of phenol in water in the presence of G3-dendr-SiO_2-Ru catalyst under various conditions at substrate/Ru of 754–887, Table S4: Hydrogenation of phenol in water in the presence of G2-dendr-*meso*-SiO_2-Ru catalyst, Table S5: Hydrogenation of alkyl-substituted phenols in the presence of G2-dendr-*meso*-SiO_2-Ru, Table S6: Hydrogenation of alkyl-substituted phenols in the presence of G3-dendr-SiO_2-Ru, Table S7: Comparison of activities of G3–HMDI–Ru [57] and G3-dendr-SiO_2-Ru in hydrogenation of alkyl-substituted phenols.

Acknowledgments: This work was supported by the Russian Foundation for Basic Research, project No. 16-33-60101 mol_a_dk.

Author Contributions: Eduard Karakhanov and Anton Maximov conceived an idea of Ru NPs, encapsulated onto PPI dendrimers, grafted onto mesoporous silica walls, and the use of them in the hydrogenation of phenol. Edile Mamedli synthesized mesoporous catalyst G2-dendr-*meso*-SiO_2-Ru, processed TEM data for it, and carried out the hydrogenation of phenol in its presence. Anna Vutolkina studied the hydrogenation kinetics of phenol in the presence of the microporous catalyst G3-dendr-SiO_2-Ru and processed TEM data for it. Andrey Ivanov provided NMR analysis of the synthesized hybrid materials. Anna Zolotukhina synthesized hybrid dendrimer-based supports, and also the microporous catalyst G3-dendr-SiO_2-Ru, carried out the hydrogenation of alkyl-substituted phenols in the presence of G3-dendr-SiO_2-Ru, processed the XPS data and wrote the paper.

Conflicts of Interest: The authors declare no conflict of interest.

References

1. Weissermel, K.; Arpe, H.-J. *Industrial Organic Chemistry*; Wiley-VCH Verlag GmbH & Co. KGaA: Weinheim, Germany, 1993; p. 457.
2. Xiang, Y.; Ma, L.; Lu, C.; Zhang, Q.; Li, X. Aqueous system for the improved hydrogenation of phenol and its derivatives. *Green Chem.* **2008**, *10*, 939–943. [CrossRef]
3. Sulman, E.M.; Ivanov, A.A.; Chernyavsky, V.S.; Sulman, M.G.; Bykov, A.I.; Sidirov, A.I.; Doluda, V.Y.; Matveeva, V.G.; Bronstein, L.M.; Stein, B.D.; et al. Kinetics of phenol hydrogenation over Pd-containing hypercrosslinked polystyrene. *Chem. Eng. J.* **2011**, *176–177*, 33–41. [CrossRef]
4. Chen, Z.; He, J.; Lemonidou, A.A.; Li, X.; Lercher, J.A. Aqueous-phase hydrodeoxygenation of bio-derived phenols to cycloalkanes. *J. Catal.* **2011**, *280*, 8–16.
5. Güvenatam, B.; Kurşun, O.; Heeres, E.H.J.; Pidko, E.A.; Hensen, E.J.M. Hydrodeoxygenation of mono- and dimeric lignin model compounds on noble metal catalysts. *Catal. Today* **2014**, *233*, 83–91.
6. Nishimura, Sh. *Handbook of Heterogeneous Catalytic Hydrogenation for Organic Synthesis*; JOHN WILEY & SONS, INC.: New York, NY, USA, 2001; pp. 427–441.
7. Karakhanov, E.A.; Dedov, A.G.; Tskhai, L.E.; Shatalov, V.V. Hydrogenation of oxygen-containing functionalized derivates of aromatic hydrocarbons. *Petrol. Chem.* **1993**, *33*, 202–227.
8. Wang, H.; Zhao, F.; Fujita, S.; Arai, M. Hydrogenation of phenol in $scCO_2$ over carbon nanofiber supported Rh catalyst. *Catal. Commun.* **2008**, *9*, 362–368. [CrossRef]

9. Itoh, N.; Xu, W.-C. Selective hydrogenation of phenol to cyclohexanone using palladium-based membranes as catalysts. *Appl. Catal. A* **1993**, *107*, 83–100. [CrossRef]
10. Ipatiev, V.N. Catalytic reactions under high pressures and temperatures. *J. Russ. Phys. Chem. Soc.* **1906**, *38*, 75–92.
11. Sabatier, P. *Catalysis in Organic Chemistry*; Goschimtechizdat: Leningrad, Soviet Union, 1932; p. 418, (translated in Russian from: Sabatier, P. Die Katalyse in der organischen Chemie, 2. A. Finkelstein, B.; Häuber, H., Eds.; Akademische Verlagsgesellschaft: Leipzig, Germany, 1927; S. 466).
12. Sandescu, N.; Grigoras, D.; Bozga, P. Catalytic Manufacture of Cyclohexanone. Rom. Patent 91,636, 30 May 1987.
13. Gutierrez-Ortiz, J.I.; Gonzalez-Velasco, J.R.; Salvador, A.R.; Gonzalez-Marcos, J.A. Etapas de transporte en la hidrogenación catalitica del fenol. II. Gradientes intraparticulares. *Afinidad* **1986**, *43*, 173–177.
14. Baltz, H.; Blume, H.; Lunau, J.; Meye, H.; Oberender, H.; Schäfer, H.; Timm, D. Cyclohexanone by Catalytic Hydrogenation of Phenol. GDR Patent 2,059,938, 8 July 1971.
15. Gonzalez-Velasco, J.R.; Gutierrez-Ortiz, J.I.; Gonzalez-Marcos, J.A.; Romero, A. Kinetics of the selective hydrogenation of phenol to cyclohexanone over a Pd-alumina catalyst. *React. Kinet. Catal. Lett.* **1986**, *32*, 505–512. [CrossRef]
16. Shono, S.; Itabashi, K.; Yamada, M.; Kikuchi, M. Catalytic hydrogenation of organic compounds by Mo trisulfide. *Kogyo Kagaku Zasshi* **1961**, *64*, 1357–1361. [CrossRef]
17. Rode, C.V.; Joshi, U.D.; Sato, O.; Shirai, M. Catalytic ring hydrogenation of phenol under supercritical carbon dioxide. *Chem. Commun.* **2003**. [CrossRef]
18. Spagovsky, Y.S.; Strelets, M.M.; Borisov, V.V. *Kinetics of Phenol Hydrogenation on Palladium and Nickel*; Siberian Department of USSR Academy of Sciences: Novosibirsk, Russia, 1973; pp. 73–80.
19. Li, H.; Liu, J.; Li, H. Liquid-phase selective hydrogenation of phenol to cyclohexanone over the Ce-doped Pd–B amorphous alloy catalyst. *Mat. Lett.* **2008**, *62*, 297–300. [CrossRef]
20. Maegawa, T.; Akashi, A.; Yaguchi, K.; Iwasaki, Y.; Shigetsura, M.; Monguchi, Y.; Sajiki, H. Efficient and practical arene hydrogenation by heterogeneous catalysts under mild conditions. *Chem. Eur. J.* **2009**, *15*, 6953–6963. [CrossRef] [PubMed]
21. Mahata, N.; Raghavan, K.V.; Vishwanathan, V.; Park, C.; Keane, M.A. Phenol hydrogenation over palladium supported on magnesia: Relationship between catalyst structure and performance. *Phys. Chem. Chem. Phys.* **2001**, *3*, 2712–2719. [CrossRef]
22. Matos, J.; Corma, A. Selective phenol hydrogenation in aqueous phase on Pd-based catalysts supported on hybrid TiO_2-carbon materials. *Appl. Catal. A* **2011**, *404*, 103–112. [CrossRef]
23. Pérez, Y.; Fajardo, M.; Corma, A. Highly selective palladium supported catalyst for hydrogenation of phenol in aqueous phase. *Catal. Commun.* **2011**, *12*, 1071–1074. [CrossRef]
24. Grasshoff, E.; Hoerinklee, W.; Kojda, P. Cyclohexanone and Cyclohexanol. GDR Patent 218,092 A2, 30 January 1985.
25. Grasshoff, E.; Meye, H.; Naumann, H. Selective Hydrogenation of Phenol to Cyclohexanone. GDR Patent 150,999, 30 September 1981.
26. Murtha, T.P. Selective Hydrogenation of Organic Materials. U.S. Patent 4,409,401, 11 October 1983.
27. Van Peppen, J.F.; Fisher, W.B. Cyclohexanone. Can. Patent 1,127,139 A2, 6 July 1982.
28. Van Peppen, J.F.; Fisher, W.B. Process for Producing Cyclohexanone. U.S. Patent 4,200,553, 29 April 1980.
29. Rossi, L.M.; Machado, G. Ruthenium nanoparticles prepared from ruthenium dioxide precursor: Highly active catalyst for hydrogenation of arenes under mild conditions. *J. Mol. Catal. A* **2009**, *298*, 69–73. [CrossRef]
30. Ponomarev, A.A.; Chegolya, A.S.; Smirnova, N.S. Liquid-phase hydrogenation of some monocyclic aromatic compounds in the presence of Ru catalysts. *Russ. Chem. Bull. Chem.* **1965**, *163*, 379–382.
31. Karakhanov, E.A.; Dedov, A.G.; Loktev, A.S.; Pshezhetsky, V.S. A Method of Cyclohexanol Obtaining. USSR Patent 1,051,056 A1, 30 October 1983.
32. Pomogailo, A.D. *Catalysis by Polymer-Immobilized Metal Complexes*; Nauka: Moscow, Russia, 1991; p. 448, CRC Press, Taylor & Francis Group: Abingdon, UK, 1999; p. 424.
33. Bekturov, E.A.; Kudaibergenov, S.E. *Catalysis by Polymers*; Wiley-VCH Verlag GmbH & Co. KGaA: Weinheim, Germany, 2002; pp. 67–144.
34. Tskhai, L.E.; Syshchikov, I.G.; Evseev, A.M. About mechanism of phenol hydrogenation on soluble metal-polymer catalysts. *Moscow Univ. Chem. Bull.* **1992**, *33*, 356–360.

35. Perchenko, V.N.; Kalashnikova, I.S.; Kamneva, G.L. Hydrogenation of phenol and its derivates on polymeric metal complexes of palladium and rhodium. *Petrol. Chem.* **1987**, *27*, 219–222.
36. Bayer, E.; Schumann, W. Liquid phase polymer-based catalysis for stereo- and regio-selective hydrogenation. *J. Chem. Soc. Chem. Commun.* **1986**, *12*, 949–952. [CrossRef]
37. Lu, F.; Liu, J.; Xu, J. Synthesis of chain-like Ru nanoparticle arrays and its catalytic activity for hydrogenation of phenol in aqueous media. *Mater. Chem. Phys.* **2008**, *108*, 369–374. [CrossRef]
38. Maksimov, A.L.; Kuklin, S.N.; Kardasheva, Y.S.; Karakhanov, E.A. Hydrogenation of phenols in ionic liquids on rhodium nanoparticles. *Petrol. Chem.* **2013**, *53*, 157–163. [CrossRef]
39. Kuklin, S.; Maximov, A.; Zolotukhina, A.; Karakhanov, E. New approach for highly selective hydrogenation of phenol to cyclohexanone: Combination of rhodium nanoparticles and cyclodextrins. *Catal. Commun.* **2016**, *73*, 63–68. [CrossRef]
40. Pittelkow, M.; Moth-Poulsen, K.; Boas, U.; Christensen, J.B. Poly(amidoamine)-dendrimer-stabilized Pd(0) nanoparticles as a catalyst for the Suzuki reaction. *Langmuir* **2003**, *19*, 7682–7684. [CrossRef]
41. Karakhanov, E.A.; Maksimov, A.L.; Zolotukhina, A.V.; Kardasheva, Y.S. Hydrogenation catalysts based on metal nanoparticles stabilized by organic ligands. *Russ. Chem. Bull.* **2013**, *62*, 1465–1492. [CrossRef]
42. Pertici, P.; Vitulli, G.; Carclini, C.; Clardelli, F. Versatile polystyrene-ruthenium hydrogenation catalysts. *J. Mol. Catal.* **1981**, *11*, 353–364. [CrossRef]
43. Maximov, A.; Zolotukhina, A.; Kulikov, L.; Kardasheva, Yu.; Karakhanov, E. Ruthenium catalysts based on mesoporous aromatic frameworks for the hydrogenation of arenes. *React. Kinet. Mech. Cat.* **2016**, *117*, 729–743. [CrossRef]
44. Raspolli Galletti, A.M.; Antonetti, C.; Longo, I.; Capannelli, G.; Venezia, A.M. A novel microwave assisted process for the synthesis of nanostructured ruthenium catalysts active in the hydrogenation of phenol to cyclohexanone. *Appl. Catal. A* **2008**, *350*, 46–52. [CrossRef]
45. Zhou, X.; Wu, T.; Hu, B.; Jiang, T.; Han, B. Ru nanoparticles stabilized by poly(*N*-vinyl-2-pyrrolidone) grafted on to silica: Very active and stable catalysts for hydrogenation of aromatics. *J. Mol. Catal. A* **2009**, *306*, 143–148. [CrossRef]
46. Wang, Y.; Yao, J.; Li, H.; Su, D.; Antonietti, M. Highly selective hydrogenation of phenol and derivatives over a Pd@carbon nitride catalyst in aqueous media. *J. Am. Chem. Soc.* **2011**, *133*, 2362–2365. [CrossRef] [PubMed]
47. Allen, J.; Rosenberg, E.; Karakhanov, E.; Kardashev, S.V.; Maximov, A.; Zolotukhina, A. Catalytic properties of transition metal salts immobilized on nanoporous silica polyamine composites II: Hydrogenation. *Appl. Organometal. Chem.* **2011**, *25*, 245–254. [CrossRef]
48. Karakhanov, E.; Maximov, A.; Kardashev, S.; Kardasheva, Yu.; Zolotukhina, A.; Rosenberg, E.; Allen, J. Nanostructured macromolecular metal containing materials in catalysis. *Macromol. Symp.* **2011**, *304*, 55–64. [CrossRef]
49. Long, W.; Brunelli, N.A.; Didas, S.A.; Ping, E.W.; Jones, C.W. Aminopolymer–silica composite-supported Pd catalysts for selective hydrogenation of alkynes. *ACS Catal.* **2013**, *3*, 1700–1708. [CrossRef]
50. Karaki, M.; Karout, A.; Toufaily, J.; Rataboul, F.; Essayem, N.; Lebeau, B. Synthesis and characterization of acidic ordered mesoporous organosilica SBA-15: Application to the hydrolysis of cellobiose and insight into the stability of the acidic functions. *J. Catal.* **2013**, *305*, 204–216. [CrossRef]
51. Ishito, N.; Kobayashi, H.; Nakajima, K.; Maegawa, Y.; Inagaki, Sh.; Hara, K.; Fukuoka, A. Ruthenium-immobilized periodic mesoporous organosilica: Synthesis, characterization, and catalytic application for selective oxidation of alkanes. *Chem. Eur. J.* **2015**, *21*, 15564–15569. [CrossRef] [PubMed]
52. Garcia-Martinez, J.; Linares, N.; Sinibaldi, S.; Coronado, E.; Ribera, A. Incorporation of Pd nanoparticles in mesostructured silica. *Micropor. Mesopor. Mater.* **2009**, *117*, 170–177. [CrossRef]
53. Garcia, R.A.; van Grieken, R.; Iglesias, J.; Morales, V.; Villajos, N. Facile one-pot approach to the synthesis of chiral periodic mesoporous organosilicas SBA-15-type materials. *J. Catal.* **2010**, *274*, 221–227. [CrossRef]
54. Newkome, G.R.; Shreiner, C.D. Poly(amidoamine), polypropylenimine, and related dendrimers and dendrons possessing different 1 → 2 branching motifs: An overview of the divergent procedures. *Polymer* **2008**, *49*, 1–173. [CrossRef]
55. Niu, Y.; Crooks, R.M. Dendrimer-encapsulated metal nanoparticles and their applications to catalysis. *C. R. Chim.* **2003**, *6*, 1049–1059. [CrossRef]
56. Karakhanov, E.A.; Maximov, A.L.; Skorkin, V.A.; Zolotukhina, A.V.; Smerdov, A.S.; Tereshchenko, A.Yu. Nanocatalysts based on dendrimers. *Pure Appl. Chem.* **2009**, *81*, 2013–2023. [CrossRef]

57. Maximov, A.; Zolotukhina, A.; Murzin, V.; Karakhanov, E.; Rosenberg, E. Ruthenium nanoparticles stabilized in cross-linked dendrimer matrices: Hydrogenation of phenols in aqueous media. *ChemCatChem* **2015**, *7*, 1197–1210. [CrossRef]
58. Karakhanov, E.A.; Maximov, A.L.; Zolotukhina, A.V.; Terenina, M.V.; Vutolkina, A.V. Nanoheterogeneous ruthenium-containing catalysts based on dendrimers in the hydrogenation of aromatic compounds under two-phase conditions. *Petrol. Chem.* **2016**, *56*, 491–502. [CrossRef]
59. Zakharyan, E.M.; Ma, G.; Maksimov, A.L.; Karakhanov, E.A.; Voronina, Z.D. Phenol and dihydroxybenzene hydrogenation catalysts based on polyamide dendrimers and rhodium species. *Petrol. Chem.* **2014**, *54*, 412–419. [CrossRef]
60. Buil, M.L.; Esteruelas, M.A.; Niembro, S.; Oliván, M.; Orzechowski, L.; Pelayo, C.; Vallribera, A. Dehalogenation and hydrogenation of aromatic compounds catalyzed by nanoparticles generated from rhodium bis(imino)pyridine complexes. *Organometallics* **2010**, *29*, 4375–4383. [CrossRef]
61. Karakhanov, E.; Maximov, A.; Zolotukhina, A.; Kardasheva, Yu.; Talanova, M. Thermo-responsive ruthenium dendrimer-based catalysts for hydrogenation of the aromatic compounds and phenols. *J. Inorg. Organomet. Polym. Mater.* **2016**, *26*, 1264–1279. [CrossRef]
62. Fairlie, D.P.; Jackson, W.G. Nitrogen- and oxygen-bonded urethane: hydrolysis and linkage isomerization of $[(NH_3)_5Co(NH_2CO_2C_2H_5)]^{3+}$ and $[(NH_3)_5CoOC(NH_2)OCH_2CH_3]^{3+}$. *Inorg. Chem.* **1990**, *29*, 3139–3145. [CrossRef]
63. Karakhanov, E.; Maximov, A.; Kardasheva, Yu.; Semernina, V.; Zolotukhina, A.; Ivanov, A.; Abbott, G.; Rosenberg, E.; Vinokurov, V. Pd Nanoparticles in dendrimers immobilized on silica-polyamine composites as catalysts for selective hydrogenation. *ACS Appl. Mater. Interfaces* **2014**, *6*, 8807–8816. [CrossRef] [PubMed]
64. Zweni, P.P.; Alper, H. Silica-supported dendrimer-palladium complex-catalyzed selective hydrogenation of dienes to monoolefins. *Adv. Synth. Catal.* **2006**, *348*, 725–731. [CrossRef]
65. Hagiwara, H.; Sasaki, H.; Tsubokawa, N.; Hoshi, T.; Suzuki, T.; Tsuda, T.; Kuwabata, S. Immobilization of Pd on nanosilica dendrimer as SILC: Highly active and sustainable cluster catalyst for Suzuki–Miyaura reaction. *SynLett.* **2010**, *13*, 1990–1996. [CrossRef]
66. Xu, Y.; Zhang, Z.; Zheng, J.; Du, Q.; Li, Yi. Synthesis of dendrimers terminated by DABCO ligands and applications of its palladium nanoparticles for catalyzing Suzuki–Miyaura and Mizoroki–Heck couplings. *Appl. Organometal. Chem.* **2013**, *27*, 13–18. [CrossRef]
67. Jiang, Y.; Gao, Q. Heterogeneous hydrogenation catalyses over recyclable Pd(0) nanoparticle catalysts stabilized by PAMAM-SBA-15 organic-inorganic hybrid composites. *J. Am. Chem. Soc.* **2006**, *128*, 716–717. [CrossRef] [PubMed]
68. Zheng, Z.; Li, H.; Liu, T.; Cao, R. Monodisperse noble metal nanoparticles stabilized in SBA-15: Synthesis, characterization and application in microwave-assisted Suzuki–Miyaura coupling reaction. *J. Catal.* **2010**, *270*, 268–274. [CrossRef]
69. Andrés, R.; de Jesús, E.; Flores, J.C. Catalysts based on palladium dendrimers. *New J. Chem.* **2007**, *31*, 1161–1191. [CrossRef]
70. Antonels, N.C.; Williams, M.B.; Meijboom, R.; Haumann, M. Well-defined dendrimer encapsulated ruthenium SCILL catalysts for partial hydrogenation of toluene in liquid-phase. *J. Mol. Catal. A* **2016**, *421*, 156–160. [CrossRef]
71. Hoover, N.N.; Auten, B.J.; Chandler, B.D. Tuning supported catalyst reactivity with dendrimer-templated Pt−Cu nanoparticles. *J. Phys. Chem. B* **2006**, *110*, 8606–8612. [CrossRef] [PubMed]
72. Kumar, P.A.; Ha, H.P. Synthesis and dispersion of dendrimer-encapsulated Pt nanoparticles on γ-Al_2O_3 for the reduction of NO_x by methane. *Catal. Lett.* **2010**, *136*, 177–184. [CrossRef]
73. Liu, D.X.; Lopez de Jesus, Y.M.; Monnier, J.R.; Williams, C.T. Preparation, characterization, and kinetic evaluation of dendrimer-derived bimetallic Pt–Ru/SiO_2 catalysts. *J. Catal.* **2010**, *269*, 376–387. [CrossRef]
74. Nefedov, V.I.; Salyn, Y.V.; Leonhardt, G.; Scheibe, R. A comparison of different spectrometers and charge corrections used in X-ray photoelectron spectroscopy. *J. Electron Spectrosc. Relat. Phenom.* **1977**, *10*, 121–124. [CrossRef]
75. Gross, T.; Ramm, M.; Sonntag, H.; Unger, W.; Meijers, H.M.; Adem, E.H. An XPS analysis of different SiO_2 modifications employing a C 1s as well as an Au $4f_{7/2}$ static charge reference. *Surf. Interface Anal.* **1992**, *18*, 59–64. [CrossRef]

76. Beamson, G.; Briggs, D. *High Resolution XPS of Organic Polymers: The Scienta ESCA300 Database*; John Wiley & Sons: Chichester, UK, 1992; p. 295.
77. Briggs, D.; Beamson, G. Primary and secondary oxygen-induced C 1s binding energy shifts in X-ray photoelectron spectroscopy of polymers. *Anal. Chem.* **1992**, *64*, 1729–1736. [CrossRef]
78. Strohmeier, B.R. Evaluation of polymeric standard reference materials for monitoring the performance of X-ray photoelectron spectrometers. *Appl. Surf. Sci.* **1991**, *47*, 225–234. [CrossRef]
79. Pertsin, A.J.; Gorelova, M.M.; Levin, V.Y.; Makarova, L.I. An XPS study of the surface–bulk compositional differences in siloxane-containing block copolymers and polymer blends. *J. Appl. Polym. Sci.* **1992**, *45*, 1195–1202. [CrossRef]
80. Laoharojanaphand, P.; Lin, T.J.; Stoffer, J.O. Glow discharge polymerization of reactive functional silanes on poly(methyl methacrylate). *J. Appl. Polymer Sci.* **1990**, *40*, 369–384. [CrossRef]
81. Zhao, D.; Huo, Q.; Feng, J.; Chmelka, B.F.; Stucky, G.D. Nonionic triblock and star diblock copolymer and oligomeric surfactant syntheses of highly ordered, hydrothermally stable, mesoporous silica structures. *J. Am. Chem. Soc.* **1998**, *120*, 6024–6036. [CrossRef]
82. Corriu, R.J.P.; Lancelle-Beltran, E.; Mehdi, A.; Reyé, C.; Brandès, S.; Guilard, R. Ordered mesoporous hybrid materials containing cobalt(II) Schiff base complex. *J. Mater. Chem.* **2002**, *12*, 1355–1362. [CrossRef]
83. Karakhanov, E.A.; Maximov, A.L.; Zolotukhina, A.V.; Kardashev, S.V. Design of dendrimer-based nanostructured catalyst systems and their catalytic activity in hydrogenation: Synthesis of ruthenium nanoparticles immobilized in dendrimer networks. *Petrol. Chem.* **2010**, *50*, 290–297. [CrossRef]
84. Charan, P.H.K.; Rao, G.R. Synthesis of CuNi and CuNi/SBA-15 by aqueous method at room temperature and their catalytic activity. *Micropor. Mesopor. Mater.* **2014**, *200*, 101–109. [CrossRef]
85. Kalbasi, R.J.; Zamani, F. Synthesis and characterization of Ni nanoparticles incorporated into hyperbranched polyamidoamine–polyvinylamine/SBA-15 catalyst for simple reduction of nitro aromatic compounds. *RSC Adv.* **2014**, *4*, 7444–7453. [CrossRef]
86. Irum, M.; Zaheer, M.; Friedrich, M.; Kempe, R. Mesoporous silica nanosphere supported platinum nanoparticles (Pt@MSN): One-pot synthesis and catalytic hydrogen generation. *RSC Adv.* **2016**, *6*, 10438–10441. [CrossRef]
87. Hughes, M.A.; Nielsen, D.; Rosenberg, E.; Gobetto, R.; Viale, A.; Burton, S.D.; Ferel, J. Structural investigations of silica polyamine composites: Surface coverage, metal ion coordination, and ligand modification. *Ind. Eng. Chem. Res.* **2006**, *45*, 6538–6547. [CrossRef]
88. González, B.; Colilla, M.; López de Laorden, C.; Vallet-Regí, M. A novel synthetic strategy for covalently bonding dendrimers to ordered mesoporous silica: Potential drug delivery applications. *J. Mater. Chem.* **2009**, *19*, 9012–9024. [CrossRef]
89. Shen, J.Y.; Adnot, A.; Kaliaguine, S. An ESCA study of the interaction of oxygen with the surface of ruthenium. *Appl. Surf. Sci.* **1991**, *51*, 47–60. [CrossRef]
90. Folkesson, B. ESCA studies on the charge distribution in some dinitrogen complexes of rhenium, iridium, ruthenium, and osmium. *Acta Chem. Scand.* **1973**, *27*, 287–302. [CrossRef]
91. Kim, K.S.; Winograd, N. X-ray photoelectron spectroscopic studies of ruthenium-oxygen surfaces. *J. Catal.* **1974**, *35*, 66–72. [CrossRef]
92. Nefedov, V.I. An influence of the oxidation degree of transition element on its X-ray photoelectron spectra. *Russ. J. Coord. Chem.* **1978**, *4*, 1283–1291.
93. Kim, Y.I.; Hatfield, W.E. Electrical, magnetic and spectroscopic properties of tetrathiafulvalene charge transfer compounds with iron, ruthenium, rhodium and iridium halides. *Inorg. Chim. Acta* **1991**, *188*, 15–24. [CrossRef]
94. Khan, M.M.T.; Srivastava, S. Some new ruthenium(III) schiff base complexes: A photoelectron spectroscopic study. *Polyhedron* **1988**, *7*, 1063–1065. [CrossRef]
95. Shepherd, R.E.; Proctor, A.; Henderson, W.W.; Myser, T.K. Assessment of the π-acceptor capability of selected ligands based on the photoelectron spectra of ruthenium ammine complexes. *Inorg. Chem.* **1987**, *26*, 2440–2444. [CrossRef]
96. Okal, J. The interaction of oxygen with high loaded Ru/γ-Al_2O_3 catalyst. *Mater. Res. Bull.* **2009**, *44*, 318–323. [CrossRef]
97. Hosokawa, S.; Kanai, H.; Utani, K.; Taniguchi, Y.; Saito, Y.; Imamura, S. State of Ru on CeO_2 and its catalytic activity in the wet oxidation of acetic acid. *Appl. Catal. B* **2003**, *45*, 181–187. [CrossRef]

98. Toyoshima, I.; Somorjai, G.A. Heats of chemisorption of O_2, H_2, CO, CO_2, and N_2 on polycrystalline and single crystal transition metal surfaces. *Catal. Rev. Sci. Eng.* **1979**, *19*, 105–159. [CrossRef]
99. Chaston, J.C. Reactions of oxygen with the platinum metals. *Platinum Met. Rev.* **1965**, *9*, 51–56.
100. Koopman, P.G.J. Ruthenium Hydrogenation Catalysts. Activation Characterization Application. Ph.D. Thesis, Delft University, Delft, The Netherlands, 1980.
101. Rylander, P.N.; Rakoncza, N.; Steele, D.; Bolliger, M. Water as co-catalyst in Ru hydrogenation. *Engelhard Ind. Tech. Bull.* **1963**, *4*, 95–100.
102. Gual, A.; Axet, M.R.; Philippot, K.; Chaudret, B.; Denicourt-Nowicky, A.; Roucoux, A.; Castillón, S.; Claver, C. Diphosphite ligands derived from carbohydrates as stabilizers for ruthenium nanoparticles: Promising catalytic systems in arene hydrogenation. *Chem. Commun.* **2008**. [CrossRef]
103. Nie, Y.; Jaenicke, S.; van Bekkum, H.; Chuah, G.-K. Stereoselective cascade hydrogenation of 4-*tert*-butylphenol and *p*-cresol over Zr-zeolite beta-supported rhodium. *J. Catal.* **2007**, *246*, 223–231. [CrossRef]
104. Hiyoshi, N.; Rode, C.V.; Sato, O.; Tetsuka, H.; Shirai, M. Stereoselective hydrogenation of *tert*-butylphenols over charcoal-supported rhodium catalyst in supercritical carbon dioxide solvent. *J. Catal.* **2007**, *252*, 57–68. [CrossRef]
105. Fihri, A.; Bouhrara, M.; Patil, U.; Cha, D.; Saih, Y.; Polshettiwar, V. Fibrous nano-silica supported ruthenium (KCC-1/Ru): A sustainable catalyst for the hydrogenolysis of alkanes with good catalytic activity and lifetime. *ACS Catal.* **2012**, *2*, 1425–1431. [CrossRef]
106. Ornelas, C.; Ruiz Aranzaes, J.; Salmon, L.; Astruc, D. "Click" dendrimers: Synthesis, redox sensing of $Pd(OAc)_2$, and remarkable catalytic hydrogenation activity of precise Pd nanoparticles stabilized by 1,2,3-triazole-containing dendrimers. *Chem. Eur. J.* **2008**, *14*, 50–64. [CrossRef] [PubMed]
107. Ooe, M.; Murata, M.; Mizugaki, T.; Ebitani, K.; Kaneda, K. Dendritic nanoreactors encapsulating Pd particles for substrate-specific hydrogenation of olefins. *NanoLett.* **2002**, *2*, 999–1002. [CrossRef]
108. de Brabander-van den Berg, E.M.M.; Meijer, E.W. Poly(propylene imine) dendrimers: Large-scale synthesis by hetereogeneously catalyzed hydrogenations. *Angew. Chem. Int. Ed.* **1993**, *32*, 1308–1311. [CrossRef]
109. Banks, C.V.; O'Laughlin, J.W. Spectrophotometric determination of ruthenium with 1,10-phenanthroline. *Anal. Chem.* **1957**, *29*, 1412–1417. [CrossRef]
110. Xu, J.; Sun, L.; Li, J.; Liang, J.; Zhang, H.; Yang, W. FITC and $Ru(phen)_3^{2+}$ co-doped silica particles as visualized ratiometric pH indicator. *Nanoscale Res. Lett.* **2011**, *6*, 561–567. [CrossRef] [PubMed]
111. Lee, J.Y.; Yang, J.; Deivaraj, T.C.; Too, H.-P.J. A novel synthesis route for ethylenediamine-protected ruthenium nanoparticles. *Colliod. Interface Sci.* **2003**, *268*, 77–80. [CrossRef]